In situ Electrosynthesis of Anthraquinone Electrolytes in Aqueous Flow Batteries

In situ Electrosynthesis of Anthraquinone Electrolytes in Aqueous Flow Batteries

Yan Jing,[1§] Min Wu,[2§] Andrew A. Wong,[2] Eric M. Fell,[2] Shijian Jin,[2] Daniel A. Pollack,[3] Emily F. Kerr,[1] Roy G. Gordon,[*,1,2] Michael J. Aziz[*,2]

[1] Department of Chemistry and Chemical Biology, Harvard University, Cambridge, Massachusetts 02138, United States

[2] John A. Paulson School of Engineering and Applied Sciences, Harvard University, Cambridge, Massachusetts 02138, United States

[3] Department of Physics, Harvard University, Cambridge, Massachusetts 02138, United States

[§] These authors contributed equally to this work.

[*] Correspondence: gordon@chemistry.harvard.edu; maziz@harvard.edu

Abstract

We demonstrate the electrochemical oxidation of an anthracene derivative to a redox-active anthraquinone at room temperature in a flow cell without the use of hazardous oxidants or noble metal catalysts. The anthraquinone, generated *in situ*, was used as the active species in a flow battery electrolyte without further modification or purification. This potentially scalable, safe, green, and economical electrosynthetic method is also applied to another anthracene-based derivative and may be extended to other redox-active aromatics.

Introduction

Aqueous redox flow batteries (ARFBs) represent a class of devices for storing electrical energy that are especially well suited for large-scale stationary deployment.[1, 2] Vanadium redox flow batteries, the most developed ARFB technology, have been limited by the high and fluctuating price of vanadium.[3]

Anthraquinone-based aqueous redox flow batteries are considered as one class of the most promising alternatives to vanadium redox flow batteries because they can be composed of earth-abundant elements such as C, H, O, and N while providing comparable electrochemical performance.[4-9] However, reducing the production cost of anthraquinone-based electrolytes and

improving their chemical stability are two major challenges preventing them from being cost-competitive.[9-14] Many factors can influence the synthesis cost of an organic molecule, including the number, duration, complexity, and yields of the reaction steps, the reaction conditions (time, temperature, and pressure), solvent and precursor costs, the cost of waste disposal, and economies of scale. Likewise, a host of factors contributes to the stability, and by extension the long-term viability, of redox-active organics including the chemical structure, solvent conditions, applied potentials, and state of charge. Only through careful consideration of all of these factors can commercial-scale organic ARFBs be viable storage solutions. Therefore, not only is the development of a stable anthraquinone important, but the design of a potentially economical, scalable, and green synthetic route toward targeted molecules is equally significant.[11, 15]

Electrochemically-mediated synthesis (electrosynthesis) enables the replacement of hazardous oxidizing and reducing agents by electric current, or "clean" electrons, through an electrode and has attracted considerable attention for both laboratory and industrial applications in multiple fields of research.[16-21] Compared to traditional thermochemical synthesis, electrosynthesis can be significantly more environmentally benign due to reduced waste production and alternative chemicals consumed.[22, 23] However, the necessity of using specific solvents combined with supporting electrolytes, along with their subsequent separations, are some of the primary hurdles limiting the feasibility of electrosynthesis compared to thermochemical processes in many cases.[16]

As an example, anthraquinone is typically produced from anthracene, an inexpensive and abundant component of coal tar and petroleum.[24] Typically, hazardous oxidants such as cerium(IV), chromium(VI), and vanadium(V) compounds dissolved in strong acids, sometimes at elevated temperatures, are used to facilitate this thermochemical conversion.[25] To minimize the use of hazardous materials, often these consumed oxidants are electrochemically regenerated and

reused for chemical oxidations,[25-30] that is, a mediated or indirect electrochemical oxidation. However, in both thermochemical conversion and mediated (indirect) electrochemical conversion, isolating anthraquinone from these hazardous solutions can be time- and capital-intensive. Electro-oxidations of anthracene and its derivatives at ~1 mM concentration have been performed previously; however, the low concentrations of anthracene substrates and poor selectivity of the reactions have prevented the method from being synthetically useful.[31-36]

Using a scalable flow cell setup,[37] we demonstrate the capability to electrochemically oxidize water-soluble anthracenes directly to anthraquinones in electrolytes without the use of strong oxidants or catalysts, producing the desired negolyte (negative electrolyte) and ferrocyanide posolyte (positive electrolyte) *in situ*. Compared to conventional thermochemical and electrochemical methods, the new method is safe and potentially inexpensive because it eliminates both the use of hazardous oxidants and the necessity of post-synthesis isolation of the products from the supporting electrolytes. Taking advantage of a flow cell and bulk electrolysis setup, the demonstrated electrosynthetic method is amenable to both continuous and batch processing. Furthermore, we confirmed that the electrosynthetic method can also be extended to other anthracene derivatives.

3,3'-(9,10-anthraquinone-diyl)bis(3-methylbutanoic acid) (**DPivOHAQ**) was recently reported as an extremely stable and potentially inexpensive negolyte active species for organic ARFBs.[38] However, the use of CrO_3 in the synthesis can be highly toxic and explosive if produced in large scale. Figure 1a shows the synthetic route for **DPivOHAQ** in three steps: 1) Through Birch reduction, anthracene (**AC**) is converted to 9,10-dihydroanthracene (**DHAC**) at room temperature (Figure S1). 2) After a Friedel–Crafts reaction and subsequent oxidation by air in one pot, two water-soluble groups are introduced and **DHAC** is re-oxidized to an **AC** derivative (Figure S2),

forming 3,3'-(anthracene-diyl)bis(3-methylbutanoic acid) (**DPivOHAC**). The **DPivOHAC** powder was then dissolved in water by adding KOH to deprotonate the carboxylic acid groups. 3) Lastly, **DPivOHAQ** negolyte active species is produced by electrochemical oxidation in an aqueous electrolyte without the need for further purification. Figure 1b illustrates how **DPivOHAQ** and ferrocyanide active species can be produced *in situ* in the flow cell's electrosynthesis mode. These materials can directly serve as the active species in the negolyte and the posolyte, respectively, of a flow battery in the same cell as illustrated in Figure 1c.

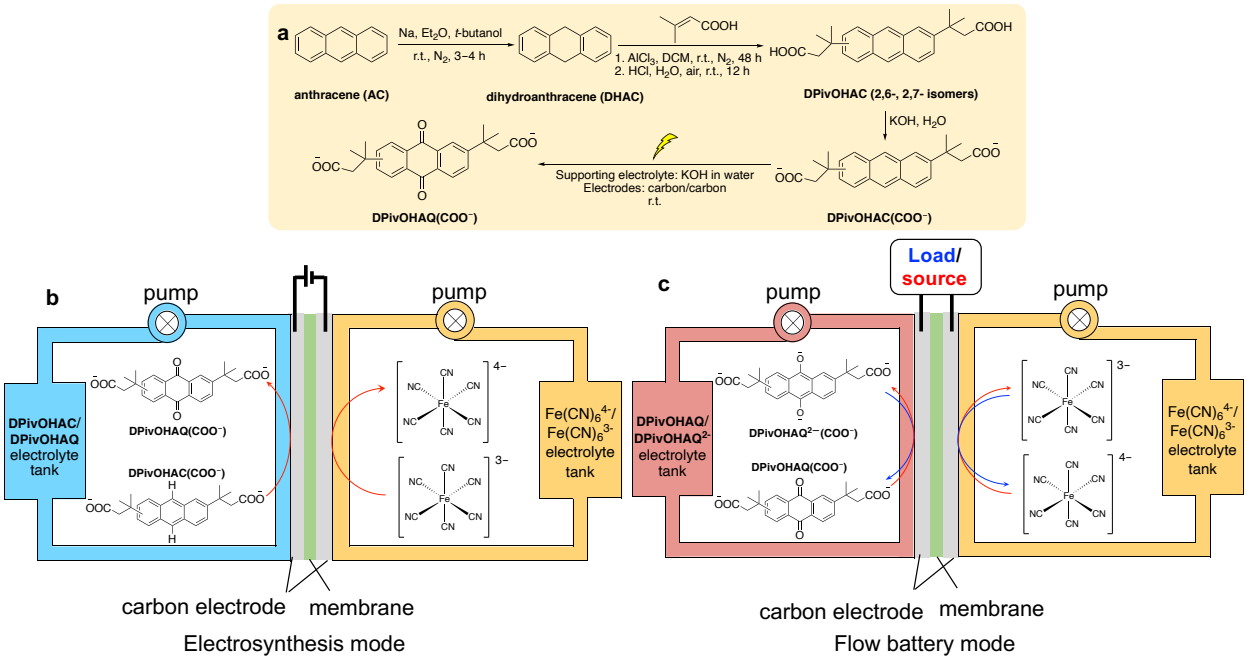

Figure 1. Preparation of DPivOHAQ and the corresponding flow battery. (a) The **DPivOHAQ** synthetic route and conditions starting from anthracene. (b) The setup for electrosynthesis of **DPivOHAQ** and ferrocyanide. (c) The flow battery setup with **DPivOHAQ** negolyte (generated *in situ*) and ferrocyanide posolyte (generated *in situ*). **DPivOHAC**: 3,3'-(anthracene-diyl)bis(3-methylbutanoic acid); **DPivOHAC(COO⁻)** is deprotonated **DPivOHAC**. **DPivOHAQ:** 3,3'-(9,10-anthraquinone-diyl)bis(3-methylbutanoic acid); **DPivOHAQ(COO⁻)** is deprotonated **DPivOHAQ.**

Figure 2a lists three different oxidation methods for **DPivOHAQ** synthesis. Conventionally, anthracene derivatives can be chemically oxidized to their anthraquinone forms by oxidants such as chromium oxide (CrO_3) in strong acidic media at elevated temperature.[38] To minimize the use

of hazardous oxidants, the strategy of mediated electrochemical oxidation can be performed by regenerating oxidants such as cerium(IV) compounds.[26, 29] However, in both of these thermochemical and indirect electrochemical oxidation processes, tedious and expensive isolation of anthraquinone-based products from oxidants and acids is required. Taking advantage of the high solubility of **DPivOHAC** in base, we demonstrate a synthetic route via direct electrochemical oxidation in alkaline electrolyte with a flow cell. This method allows the complete elimination of hazardous oxidants and costly separation processes.

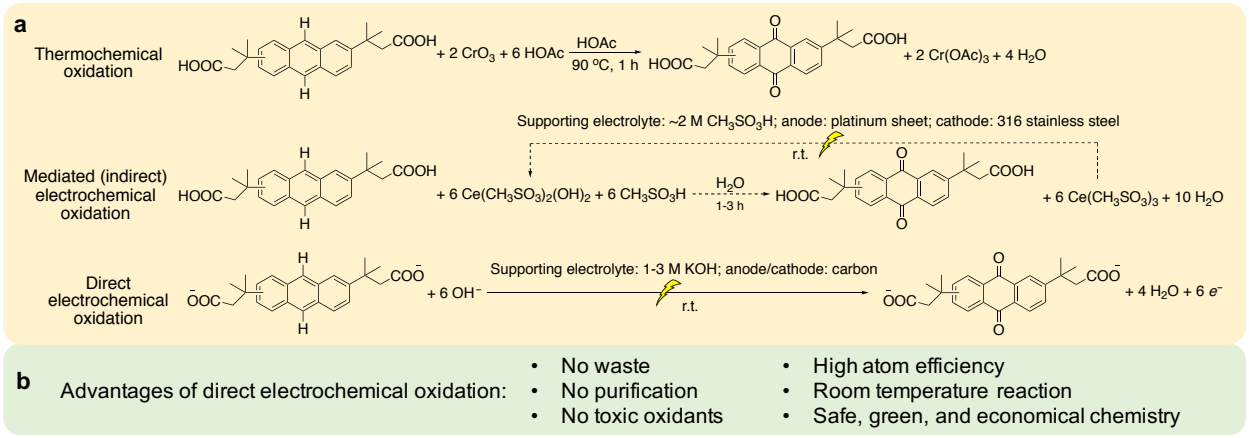

Figure 2. Comparison of DPivOHAQ synthetic methods. (a) Thermochemical, mediated (indirect) electrochemical, and direct electrochemical oxidation reactions to synthesize **DPivOHAQ**. (b) Advantages of direct electrochemical oxidation *in situ*.

Experimental

Cell hardware

Glassy carbon was used as the working electrode for all three-electrode cyclic voltammetry (CV) tests with a 5 mm diameter glassy carbon working electrode, an Ag/AgCl reference electrode (BASi, pre-soaked in 3 M NaCl solution), and a graphite counter electrode. Both undivided cell and divided cell were built for electrosynthesis. Flow battery experiments were constructed with cell hardware from Fuel Cell Tech (Albuquerque, NM) assembled into a zero-gap flow cell configuration. Pyrosealed POCO graphite flow plates with serpentine flow patterns were used for

both electrodes. Each electrode comprised a 5 cm^2 geometric surface area covered by AvCarb HCBA woven carbon fiber without pretreatment, or Pt-coated Toray carbon paper without pretreatment. The membrane is pre-soaked (1 M KOH for 24 hours) Nafion 212.

Undivided electrolytic cell setup (electrochemical oxidation vs. the HER)

Working electrode: carbon felt, where **DPivOHAC(COO^-)** was oxidized to **DPivOHAQ(COO^-)**; counter electrode: carbon rod, where water was reduced to hydrogen gas. While the electrolyte was stirred, a constant potential (1.1 V vs. Ag/AgCl) was applied to the divided electrolytic cell until 120% of the required coulombs were extracted from the working electrode.

Divided electrolytic cell setup (electrochemical oxidation vs. the ORR)

Anode: Commercial AvCarb HCBA (woven carbon cloth), where **DPivOHAC(COO^-)** was oxidized to **DPivOHAQ(COO^-)**; cathode: platinum coated Toray carbon paper, where humidified air/oxygen was reduced to hydroxide. A constant voltage (1.8 V) was applied to the divided electrolytic cell until the current decreased to 2 mA/cm^2. The number of extracted electrons was ~1.2 times higher than the theoretical value.

Divided electrolytic cell setup (electrochemical oxidation vs. the reduction of ferricyanide)

Anode: AvCarb HCBA (woven carbon cloth), where **DPivOHAC(COO^-)** was oxidized to **DPivOHAQ(COO^-)**; cathode: AvCarb HCBA (woven carbon cloth), where potassium ferricyanide was reduced to potassium ferrocyanide. A constant current density (20 mA/cm^2) was applied to the divided cell for at most 1.5 hours with a 1.2 V voltage cutoff; when either time or voltage reached the limit, the potential was held (1.2 V vs. ferro-/ferricyanide) until the current decreased to 2 mA/cm^2. The number of extracted electrons was ~1.2 times higher than the theoretical value.

An aliquot (~250 μL) was transferred from the as-prepared anolyte to an Eppendorf® tube (capacity: 1.5 mL) and acidified by a drop of concentrated HCl to obtain **DPivOHAQ** precipitate. The final **DPivOHAQ** precipitate was re-dissolved in DMSO-d_6 for ^{1}H NMR measurement. The yield was determined by peak integrations of spectrum. Faradaic efficiency (%) = yield (%) / 1.2. More detailed information can be found in the Supplementary information.

Results and Discussion

In an electrolytic cell, an anodic oxidation half reaction must be accompanied by a cathodic reduction half reaction. As shown in Table 1, we devise three different reduction half reactions to be coupled with direct **DPivOHAC** electrochemical oxidation, *i.e.*, the hydrogen evolution reaction (HER), the oxygen reduction reaction (ORR), and the $Fe(CN)_6^{3-}$ to $Fe(CN)_6^{4-}$ reduction reaction. The corresponding oxidation or reduction potentials for these reactions are listed in Table 1.

For the electrochemical oxidation of **DPivOHAC** to **DPivOHAQ**, two cell types are used, as diagramed and described in Figures S3 and S4. A divided cell uses an ion exchange membrane to separate the two half reactions, resembling the architecture of traditional fuel cells and ARFBs. An undivided cell employs two electrodes suspended in electrolyte without the use of a membrane, reflecting a bulk electrolysis cell.

Comparing these three overall reactions, the first one paired with the HER requires the highest voltage; the second one paired with the ORR is known to have slow reaction kinetics and a high overpotential;[39] the third one paired with $Fe(CN)_6^{3-}$ to $Fe(CN)_6^{4-}$ reduction exhibits the lowest overall reaction cell voltage, suggesting the least amount of energy will be required for electrosynthesis. Another merit of the third reaction is the *in situ* generation of the desired negolyte active species (**DPivOHAQ**) and posolyte active species $Fe(CN)_6^{4-}$ simultaneously. The

disadvantage is that at least six equivalents of ferricyanide and hydroxide are used. Given the similar reduction potentials of the ORR and of ferricyanide to ferrocyanide, an important direction for future research is the concurrent reduction of oxygen and ferricyanide in order to achieve high yields as well as lower ferricyanide usage. By using the same full cell configuration without changing electrolyte reservoirs, carbon-based electrodes, or ion-exchange membranes, we can immediately switch from electrosynthesis mode to flow battery mode for electrochemical energy storage. In this configuration, neither hazardous oxidants nor purification steps are needed, nor is waste generated. Furthermore, the reaction may proceed at room temperature with high atom efficiency. The new synthesis is therefore potentially safe, green, economical, and scalable.

Table 1. Anodic, cathodic, and overall reactions for direct electrochemical oxidation.

	Reactions	Potential at pH 14 (V vs SHE) / Cell voltage (V)
Anodic	**DPivOHAC(COO$^-$)** + 6 OH^- ⟶ **DPivOHAQ(COO$^-$)** + 4 H_2O + 6 e^-	1.14*
Cathodic	6 H_2O + 6 e^- ⟶ 3 H_2 + 6 OH^- (divided or undivided cell)	–0.83
	1.5 O_2 + 6 e^- + 3 H_2O ⟶ 6 OH^- (divided or undivided cell)	0.40
	6 $Fe(CN)_6^{3-}$ + 6 e^- ⟶ 6 $Fe(CN)_6^{4-}$ (divided cell)	0.44
Overall	**DPivOHAC(COO$^-$)** + 2 H_2O ⟶ **DPivOHAQ(COO$^-$)** + 3 H_2	1.97
	DPivOHAC(COO$^-$) + 1.5 O_2 ⟶ **DPivOHAQ(COO$^-$)** + H_2O	0.74
	DPivOHAC(COO$^-$) + 6 OH^- + 6 $Fe(CN)_6^{3-}$ ⟶ **DPivOHAQ(COO$^-$)** + 6 $Fe(CN)_6^{4-}$ + 4 H_2O	0.70

*: The electro-oxidation potential at peak current

The cyclic voltammogram (CV) of **DPivOHAC** at pH 14 (Figure 3a) indicates a peak oxidation current at 1.14 V vs. SHE. This value is more positive than the standard redox potential of 0.40 V vs. SHE for the oxygen evolution reaction (OER), and we expect that the OER will be a major side reaction of electrosynthesis.

We then assembled a flow cell with **DPivOHAC** as the anolyte and $K_3Fe(CN)_6$ as the catholyte. Galvanostatic electrolysis with a potentiostatic hold after reaching a potential limit of 1.2 V was performed for ~4.5 hours to complete the electrosynthesis. The OER side reaction, evidenced by

the observation of bubbles generated in the anolyte, precludes a faradaic efficiency of 100%. Thus, the number of electrons extracted from the anolyte was ~1.2 times higher than the theoretical number for complete conversion. A plateau appears at ~0.8 V against $K_3Fe(CN)_6$ (0.44 V vs. SHE) in the voltage profile (Figure 3b).

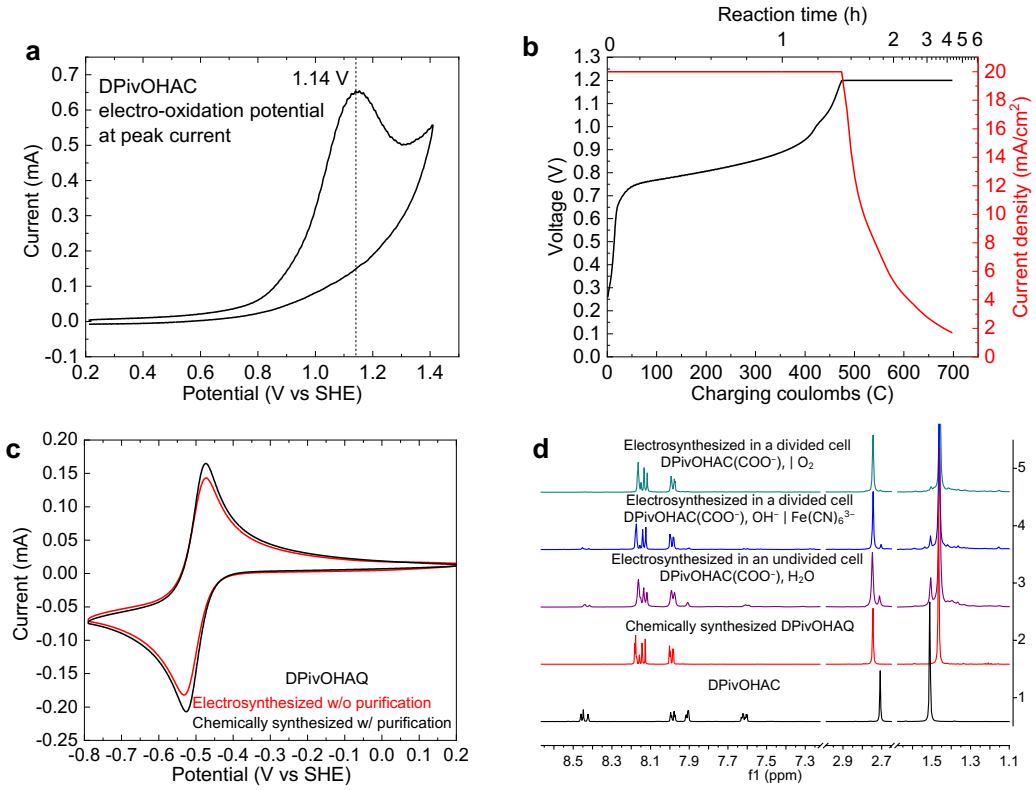

Figure 3. Electrosynthesis and characterization of DPivOHAQ. (a) The cyclic voltammogram (CV) of 0.1 M **DPivOHAC** in 1.0 M KCl + 1.0 M KOH aqueous solution. Scan rate: 0.1 V/s. (b) The electrochemical oxidation was conducted by using a constant current (20 mA/cm^2) with a subsequent potential hold (1.2 V) until the current density decreased to 2 mA/cm^2. (c) CV of 10 mM electrosynthesized **DPivOHAQ** (against $Fe(CN)_6^{3-}$) without purification and 10 mM chemically synthesized **DPivOHAQ** with purification in 1 M KOH aqueous solutions, respectively. Scan rate: 0.1 V/s. (d) ^{1}H NMR spectra of (bottom to top): chemically synthesized **DPivOHAC** (black); chemically synthesized **DPivOHAQ** (red); electrosynthesized **DPivOHAQ** in an undivided cell (purple), 17.3% of **DPivOHAC** remained unreacted according to the integration, yield: 82.7%; electro-synthesized **DPivOHAQ** in a divided cell against $Fe(CN)_6^{3-}$ (blue), 7.0% of **DPivOHAC** remained unreacted according to the integration, yield: 93.0%; electrosynthesized **DPivOHAQ** in a divided cell against O_2 (green), 0 % of **DPivOHAC** remained unreacted according to the integration, yield: 100%. The deuterated solvent is DMSO-d_6, and the solvent peaks (DMSO and H_2O) were removed to better display the peaks of interest. The

electrosynthetic details are described under the headings **Electrosynthesis I, II,** and **III** in the Supporting Information.

We compared the CV of **DPivOHAQ** produced by electrosynthesis against the reduction of $Fe(CN)_6^{3-}$ to that of the chemically synthesized product at the same concentration to verify that the reaction products are the same regardless of the synthetic procedure employed (Figure 3c). The two CV curves show identical redox peaks and similar peak currents, indicating a high-yield electrosynthesis process. ^{1}H nuclear magnetic resonance (NMR) spectroscopy was used to further examine the structure of electrosynthesized **DPivOHAQ** when using either a divided or undivided cell (Figure S3) and to compare the spectra with those of the starting material, **DPivOHAC**, and the chemically synthesized **DPivOHAQ**. The top three spectra in Figure 3d are the ^{1}H NMR spectra from electrosynthesized **DPivOHAQ**, in which the dominating peaks have the same chemical shifts as those in the spectrum of chemically synthesized **DPivOHAQ**, further suggesting the desired product was achieved.

Slightly different yields of **DPivOHAQ** were obtained when paired with the HER in an undivided cell or with $Fe(CN)_6^{3-}$ reduction or the ORR in a divided cell (Figure S4). The 82.7% yield when paired with the HER in an undivided cell could be explained by a molecular shuttling effect; *i.e.*, the electrosynthesized **DPivOHAQ** can first migrate to the cathode where it is reduced, then diffuse back to the anode for re-oxidation. As a result, double counting of electrons can occur. When paired with the $Fe(CN)_6^{3-}$ reduction half reaction, a yield of 93.0% was obtained. The incomplete yield is likely due to the consumption and therefore decreased concentration of both **DPivOHAC** and OH^- as the electrosynthesis continues, making further oxidation increasingly difficult.

The use of the ORR half reaction achieved almost 100.0% yield. This exceptional yield may be attributed to the as-formed OH^- ions on the cathode (ORR) side crossing over to the anolyte and compensating for any loss of OH^- ions on the anode side. Overall yields in excess of 80.0% for all three conditions exceed many conventional reactions and are acceptable for direct flow battery use without purification or separation.

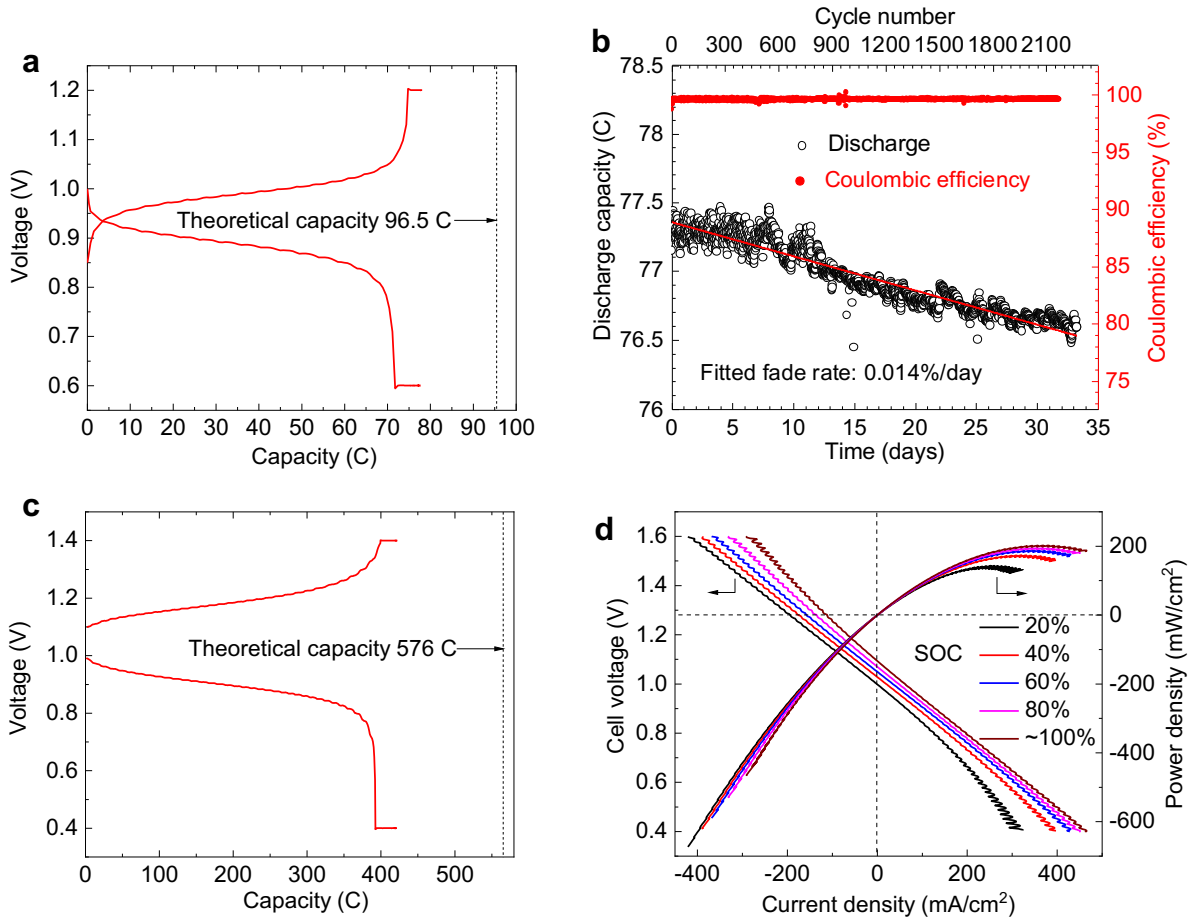

Figure 4. Full cell performance evaluation from Electrosynthesis III and IV. (a) A representative charge–discharge profile with 0.1 M **DPivOHAQ**. Negolyte: 5 mL of 0.1 M **DPivOHAQ** pH = ~13.5. Posolyte: 100 mL of 0.1 M potassium ferro-/ferricyanide solution [~0.06 M $K_4Fe(CN)_6$ and ~0.04 M $K_3Fe(CN)_6$] pH = ~13.6. (b) Discharge capacity (C) and coulombic efficiency (%) vs. cycle number and time (days). Negolyte: 4.5 mL of 0.1 M **DPivOHAQ**. Posolyte: 100 mL of 0.1 M ferro-/ferricyanide solution [~0.06 M $K_4Fe(CN)_6$ and ~0.04 M $K_3Fe(CN)_6$]. Current density: 30 mA/cm^2 with potential hold (cutoffs: 0.6 V, 1.2 V) until current decreased to 2 mA/cm^2. (c) A representative charge–discharge profile with 0.5 M **DPivOHAQ**. Negolyte: 6 mL of 0.5 M **DPivOHAQ**. Posolyte: 100 mL of 0.5 M potassium ferro-/ferricyanide solution [~0.3

M $K_4Fe(CN)_6$ and ~0.2 M $K_3Fe(CN)_6$]. Current density: 100 mA/cm^2 with potential hold (cutoff: 0.4 V, 1.4 V) until current decreased to 2 mA/cm^2. (d) Polarization curves of the 0.5 M **DPivOHAQ** at the SOC of 20%, 40%, 60%, 80%, and ~100% respectively. Descriptions of **Electrosynthesis III** and **IV** can be found in the Supporting Information.

To demonstrate the feasibility of switching from the electrosynthesis mode (when paired with $Fe(CN)_6^{3-}$ reduction) to flow battery mode, we began charge–discharge cycling immediately upon completion of the electrosynthesis, without performing any purification. Because other research has reported that quinones and related compounds can decompose in the presence of light,[40-42] we wrapped the electrolyte reservoirs with aluminum foil to avoid light-induced decomposition during cell cycling (Figures S13–S15). Figure 4a shows the charge–discharge profile of a single cycle with an open circuit voltage of ~1.0 V and a capacity of 84.0 coulombs. Given the 93.0% yield found from the ^{1}H NMR, the capacity utilization is 93.6%. Long-term cycling was then performed to determine a temporal capacity fade rate of the full cell. Figure 4b demonstrates the discharge capacity and coulombic efficiency over 33.2 days and 2271 cycles with a fitted fade rate of 0.014%/day and an average coulombic efficiency of 99.53%. This is consistent with the fade rate of chemically synthesized **DPivOHAQ**.[38] The extremely low capacity fade rate is attributed to the chemical stability of the molecular structure. The C–C covalent bond between the anthraquinone core and the functionalizing chains is more robust in strong base and at elevated temperature than the C–O bond demonstrated in previous work.[4, 5, 38] Furthermore, the two branched methyl groups on the carbon connected to the anthraquinone (AQ) core may increase the stability of the solubilizing chain even when exposed to harsh conditions.[15]

To examine the feasibility of this method for potential industry use, we further conducted electrosynthesis with a higher concentration (0.5 M) of **DPivOHAC** at a higher current density (100 mA/cm^2) (See Figure S5). Figure 4c shows that 0.5 M electrosynthesized negolyte can deliver 72.9% of the theoretical capacity. We attribute the discrepancy between the delivered capacity and

the theoretical capacity primarily to incomplete conversion (Figure S6). The capacity utilization is 81.9% if we consider that there is 11.0% unreacted **DPivOHAC(COO$^-$)** in the negolyte. Additionally, the mass transport of active species at 0.5 M concentration may be another issue limiting the full capacity utilization. The corresponding polarization curve at different states of charge (SOC) is shown in Figure 4d. The peak power density exceeds 0.2 W/cm^2 when at ~100 % of SOC.

Given the total transfer of six electrons during the electrosynthesis of **DPivOHAC** to **DPivOHAQ**, the high yields achieved in this work might be surprising. We hypothesize a three-step successive two-electron transfer mechanism[34, 35]: first, when a potential is applied, anthracene (**AC**) may react with three OH^- ions and donate two electrons to produce two water molecules and the anthrone anion (**A$^-$**); second, **A$^-$** may further react with another three OH^- ions and donate another two electrons to generate two water molecules and the deprotonated anthrahydroquinone dianion (**AQ^{2-}**); third, **AQ^{2-}** may further release two electrons to afford the anthraquinone species (**AQ**). Complete electrochemical conversion in the third step has been well-documented at negative potentials vs. ferro-/ferricyanide[1, 2, 43] and should therefore be rapid at positive potentials vs. ferro-/ferricyanide. The reverse reaction of the second step has recently been identified as a side reaction in ARFBs, and the forward reaction is chemically feasible when exposed to O_2 or air.[14, 38] Given the high voltage applied to the cell, it is thus plausible that the forward reactions (**AC** to **A$^-$** to **AQ^{2-}**/**AQ**) can electrochemically proceed completely and swiftly.

Our group has also previously proposed a side reaction pathway for anthraquinones,[14, 44] where the anthrone anion (**A$^-$**) can be oxidatively dimerized to dianthrone (**DA**) chemically and/or electrochemically. According to ^{1}H NMR spectra (Figure 3d) and liquid chromatography–mass spectrometry (LC–MS) results (Figure S7), neither **DA** nor Kolbe electrolysis-related byproducts[45]

were detected (Scheme S1), suggesting that **AC**/**AQ**-related side reactions can be negligible when a sufficient OH^- concentration is present to prevent dianthrone formation and a sufficiently low voltage cutoff is chosen to prevent Kolbe electrolysis dimer formation. The major competing side reaction is the OER, which, along with the reactions of **AC** to $\mathbf{A^-}$ to $\mathbf{AQ^{2-}}$, will consume OH^- and may lead to the formation of **DA** as a result of insufficient OH^- ions in the **DPivOHAC** solution (see **Electrosynthesis V** in the SI). Interestingly, the dianthrones (Scheme S2), detected by LC–MS (Figure S11), are surprisingly redox-active when a broad voltage window is applied (Figures S8 and S9 and Scheme S2). On the one hand, the OER can reduce faradaic efficiency; on the other hand, the generated oxygen can serve as a mediator and chemically oxidize intermediates (*i.e.*, $\mathbf{A^-}$, $\mathbf{AQ^{2-}}$) to the final **AQ** form, *i.e.*, mediated (indirect) electrochemical oxidation. Because the entire process involves not only electrochemical oxidations, but also chemical oxidations, it is more appropriate to call it an electrochemical–chemical oxidation process.[46]

In the proposed mechanism, the anthrone derivative is an intermediate in the electrochemical oxidation. Anthrone formation has been identified as the major side reaction causing capacity fade in previous work;[14, 38] therefore, it is plausible that lost capacity of anthraquinone flow battery systems may be recovered and anthraquinone lifetime extended by electrochemically oxidizing anthrone to redox-active anthraquinone derivatives.

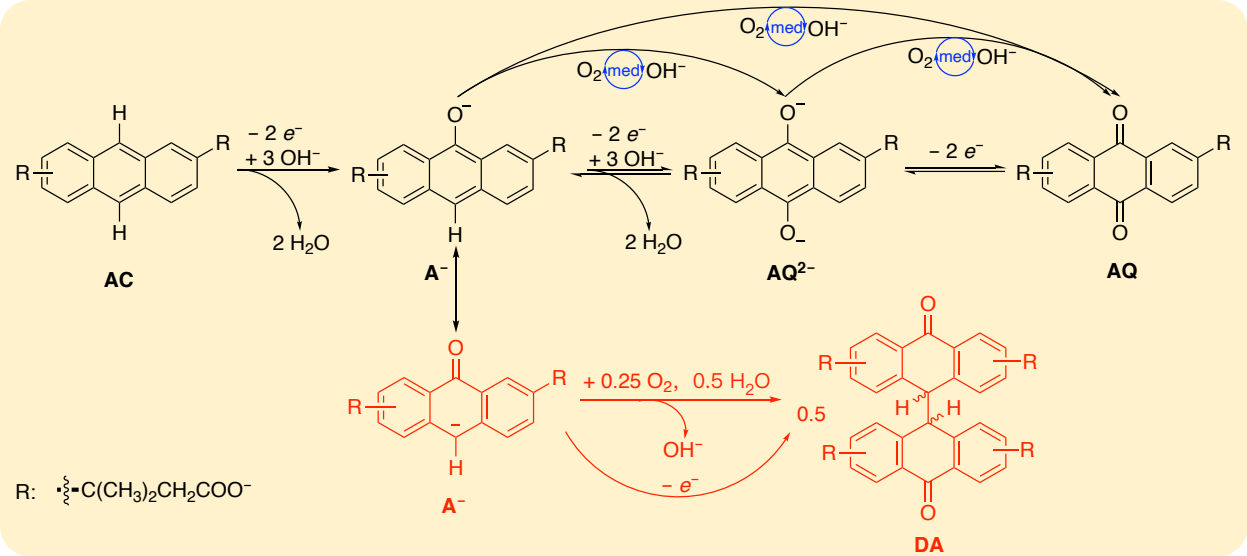

Scheme 1. Proposed electrochemical oxidation mechanism. Three-step successive two-electron transfer process from **AC** to $\mathbf{A}^{-}$, $\mathbf{A}^{-}$ to $\mathbf{AQ}^{2-}$, and $\mathbf{AQ}^{2-}$ to **AQ**. The generated oxygen from the OER side reaction may incur chemical oxidation processes including $\mathbf{A}^{-}$ to $\mathbf{AQ}^{2-}$, $\mathbf{AQ}^{2-}$ to **AQ**, and oxidative dimerization ($\mathbf{A}^{-}$ to **DA**).

To demonstrate that the electrochemical oxidation can be applied to other anthracene derivatives, we performed electrochemical oxidation of 4,4'-(9,10-dihydroanthracene-diyl)dibutanoic acid (**DBDHAC**), where the molecular core is 9,10-dihydroanthracene.[38] The ^{1}H NMR results indicate that **DBDHAC** can, like **DPivOHAC**, be electrochemically oxidized to the final anthraquinone (Figure S12), **DBAQ** (4,4'-(9,10-anthraquinone-diyl)dibutanoic acid), which has also been shown to be extremely stable.[38]

The shared precursor of **DPivOHAQ** and **DBAQ**, anthracene, is abundant in crude petroleum and coal tar, and can be synthesized from benzene and benzyl alcohol (Scheme S3).[47] The precursor of **DPivOHAQ**, 3,3'-dimethyl acrylic acid, can be industrially produced from malonic acid, a food acid; the precursor of **DBAQ**, succinic anhydride, can be industrially hydrogenated from maleic anhydride and used as an important intermediate on an industrial scale. Thus, both **DPivOHAQ** and **DBAQ** can be readily synthesized from commodity chemicals. Although the synthetic cost of **DPivOHAQ** or **DBAQ** should be somewhat higher than that of 2,6-

316 dihydroxyanthraquinone (**DHAQ**) due to more steps and more chemicals involved, the capital cost
317 of AORFBs that utilize finite-lifetime electrolytes can be viewed as including the total active cost,
318 which is the sum of the initial cost of redox-active materials and the present value of the future
319 costs of periodic electrolyte replacement.[13] This can lead to an initial cost—lifetime trade-off in
320 the choice of electrolytes. Over an extended operational lifetime, the total active cost of
321 **DPivOHAQ** or **DBAQ** may be less than that of **DHAQ** due to their much longer lifetimes.[14]
322
323 **Conclusion**

324 This work demonstrates a potentially scalable, safe, green, and economical *in situ*
325 electrosynthetic method for anthraquinone electrolytes in a flow cell without the use of hazardous
326 oxidants or precious metal catalysts. The as-generated electrolytes, which are extremely stable,
327 can be immediately used in a redox flow battery without separation or purification. Other low-cost
328 compounds may also be amenable to this approach, providing a pathway to lower the cost of
329 electrochemical grid storage systems, thereby accelerating the development of a renewable energy
330 economy. The technique extends the opportunities for direct aqueous electrosynthesis to replace
331 thermochemical synthesis of value-added organics.

332 **Supplementary Information**

333 Supplementary Information can be found with this article online at

334 **Acknowledgments**

335 This research was supported by U.S. DOE award DE-AC05-76RL01830 through PNNL
336 subcontract 428977, Innovation Fund Denmark via the Grand Solutions project "ORBATS" file
337 no. 7046-00018B, and NSF grant CBET-1914543. D.A.P. acknowledges funding support from the
338 NSF Graduate Research Fellowship Program, no. DGE1144152 and DGE1745303.

339 **Declaration of Interests**

340 Harvard University has filed a patent application on the materials and the electrosynthetic methods
341 described in this paper.

342

REFERENCES

1. B. Huskinson, M. P. Marshak, C. Suh, S. Er, M. R. Gerhardt, C. J. Galvin, X. Chen, A. Aspuru-Guzik, R. G. Gordon and M. J. Aziz, *Nature*, 2014, **505**, 195–198.
2. K. Lin, Q. Chen, M. R. Gerhardt, L. Tong, S. B. Kim, L. Eisenach, A. W. Valle, D. Hardee, R. G. Gordon, M. J. Aziz and M. P. Marshak, *Science*, 2015, **349**, 1529–1532.
3. M. Moore, R. Counce, J. Watson and T. Zawodzinski, *Journal of Advanced Chemical Engineering*, 2015, **5**, doi:10.4172/2090-4568.1000140.
4. D. G. Kwabi, K. Lin, Y. Ji, E. F. Kerr, M.-A. Goulet, D. De Porcellinis, D. P. Tabor, D. A. Pollack, A. Aspuru-Guzik, R. G. Gordon and M. J. Aziz, *Joule*, 2018, **2**, 1894–1906.
5. Y. Ji, M.-A. Goulet, D. A. Pollack, D. G. Kwabi, S. Jin, D. De Porcellinis, E. F. Kerr, R. G. Gordon and M. J. Aziz, *Adv. Energy Mater.*, 2019, **9**, 1900039.
6. A. Hollas, X. Wei, V. Murugesan, Z. Nie, B. Li, D. Reed, J. Liu, V. Sprenkle and W. Wang, *Nature Energy*, 2018, **3**, 508–514.
7. C. Wang, X. Li, B. Yu, Y. Wang, Z. Yang, H. Wang, H. Lin, J. Ma, G. Li and Z. Jin, *ACS Energy Letters*, 2020, **5**, 411–417.
8. J. D. Hofmann, F. L. Pfanschilling, N. Krawczyk, P. Geigle, L. Hong, S. Schmalisch, H. A. Wegner, D. Mollenhauer, J. Janek and D. Schröder, *Chemistry of Materials*, 2018, **30**, 762–774.
9. D. G. Kwabi, Y. Ji and M. J. Aziz, *Chem. Rev.*, 2020, **120**, doi.org/10.1021/acs.chemrev.9b00599.
10. Z. Yang, L. Tong, D. P. Tabor, E. S. Beh, M.-A. Goulet, D. De Porcellinis, A. Aspuru-Guzik, R. G. Gordon and M. J. Aziz, *Adv. Energy Mater.*, 2018, **8**, 1702056.
11. V. Dieterich, J. D. Milshtein, J. L. Barton, T. J. Carney, R. M. Darling, F. R. Brushett, *Translational Materials Research*, 2018, **5**, 034001.
12. S. Jin, E. M. Fell, L. Vina-Lopez, Y. Jing, P. W. Michalak, R. G. Gordon and M. J. Aziz, *Adv. Energy Mater.*, 2020, **10**, doi.org/10.1002/aenm.202000100.
13. F. R. Brushett, M. J. Aziz and K. E. Rodby, *ACS Energy Letters*, 2020, **5**, 879–884.
14. M.-A. Goulet, L. Tong, D. A. Pollack, D. P. Tabor, S. A. Odom, A. Aspuru-Guzik, E. E. Kwan, R. G. Gordon and M. J. Aziz, *J. Am. Chem. Soc.*, 2019, **141**, 8014–8019.
15. P. Anastas, N. Eghbali, *Chem. Soc. Rev.*, 2010, **39**, 301–312.
16. D. S. P. Cardoso, B. Šljukić, D. M. F. Santos, C. A. C. Sequeira, *Organic Process Research & Development*, 2017, **21**, 1213–1226.
17. M. Yan, Y. Kawamata, P. S. Baran, *Chem. Rev.*, 2017, **117**, 13230–13319.
18. B. K. Peters, K. X. Rodriguez, S. H. Reisberg, S. B. Beil, D. P. Hickey, Y. Kawamata, M. Collins, J. Starr, L. Chen, S. Udyavara, K. Klunder, T. J. Gorey, S. L. Anderson, M. Neurock, S. D. Minteer and P. S. Baran, *Science*, 2019, **363**, 838–845.
19. E. J. Horn, B. R. Rosen, Y. Chen, J. Tang, K. Chen, M. D. Eastgate, P. S. Baran, *Nature*, 2016, **533**, 77–81.
20. A. Badalyan, S. S. Stahl, *Nature*, 2016, **535**, 406–410.
21. G. G. Botte, *The Electrochemical Society Interface*, 2014, **23**, 49–55.
22. P. M. Bersier, L. Carlsson and J. Bersier, *Topics in Current Chemistry*, 1994, **170**, 116–136.
23. C. Xia, Y. Xia, P. Zhu, L. Fan and H. Wang, *Science*, 2019, **366**, 226–231.
24. M. Granda, C. Blanco, P. Alvarez, J. W. Patrick and R. Menendez, *Chem. Rev.*, 2014, **114**, 1608–1636.
25. R. S. Tipson, in *National Bureau of Standards Monograph 87*, 1965, 1–49.
26. R. P. Kreh, R. M. Spotnitz and J. T. Lundquist, *J. Org. Chem.,* 1989, **54**, 1531–1535.
27. E. Oppermann, *US Pat.,* US823,435A, 1906.
28. E. Steckhan, in *Ullmann's Encyclopedia of Industrial Chemistry*, Wiley-VCH Verlag GmbH & Co. KGaA, Weinheim, 2011, **12**, DOI: 10.1002/14356007.o09_o04.

29. R. M. Spotnitz, R. P. Kreh, J. T. Lundquist and P. J. Press, *Journal of Applied Electrochemistry*, 1990, **20**, 209–215.
30. R. P. Kreh, R. M. Spotnitz and J. T. Lundquist, *Tetrahedron Letters*, 1987, **28**, 1067–1068.
31. E. J. Majeski, J. D. Stuart and W. E. Ohnesorge, *J. Am. Chem. Soc.*,1968, **90**, 633–636.
32. L. R. Faulkner, A. J. Bard, *J. Am. Chem. Soc.*, 1968, **90**, 6284–6290.
33. C. Amatore and A. R. Brown, *J. Am. Chem. Soc.*, 1996, **118**, 1482–1486.
34. O. Tovide, N. Jahed, C. E. Sunday, K. Pokpas, R. F. Ajayi, H. R. Makelane, K. M. Molapo, S. V. John, P. G. Baker and E. I. Iwuoha, *Sensors and Actuators B: Chemical*, 2014, **205**, 184–192.
35. C. A. Paddon, C. E. Banks, I. G. Davies and R. G. Compton, *Ultrason. Sonochem.*, 2006, **13**, 126–132.
36. V. D. Parker, *Acta Chemica Scandinavica*, 1970, **24**, 2757–2767.
37. T. Noel, Y. Cao and G. Laudadio, *Acc. Chem. Res.*, 2019, **52**, 2858–2869.
38. M. Wu, Y. Jing, A. A. Wong, E. M. Fell, S. Jin, Z. Tang, R. G. Gordon and M. J. Aziz, *Chem*, 2020, **6**, 1432–1442.
39. R. W. Zurilla, R. K. Sen and E. Yeager, *J. Electrochem. Soc.*, 1978, **125**, 1103–1109.
40. G. Maier, L. H. Franz, H.-G. Hartan, K. Lanz and H. P. Reisenauer, *Chemische Berichte*, 1985, **118**, 3196–3204.
41. S. A. Carlson and D. M. Hercules, *Analytical Chemistry*, 1973, **45**, 1794–1799.
42. B. E. Hulme, E. J. Land and G. O. Phillips, *J. Chem. Soc. Faraday Trans. 1*, 1972, **68**, 1992–2002.
43. M. Quan, D. Sanchez, M. F. Wasylkiw and D. K. Smith, *J. Am. Chem. Soc.*, 2007, **129**, 12847–12856.
44. S. Jin, Y. Jing, D. G. Kwabi, Y. Ji, L. Tong, D. De Porcellinis, M. A. Goulet, D. A. Pollack, R. G. Gordon and M. J. Aziz, *ACS Energy Letters*, 2019, **4**, 1342–1348.
45. H.-J. Schäfer, *Topics in Current Chemistry*, 1990, **152**, 91–151.
46. C. Costentin and J.-M. Savéant, *Proc. Natl. Acad. Sci. U S A*, 2019, **116**, 11147–11152.
47. H. E. Ungnade and E. W. Crandall, *J. Am. Chem. Soc.*, 1949, **71**, 3009–3010.

Supplementary Information

In situ Electrosynthesis of Anthraquinone Electrolytes in Aqueous Flow Batteries

Yan Jing,[1§] Min Wu,[2§] Andrew A. Wong,[2] Eric M. Fell,[2] Shijian Jin,[2] Daniel A. Pollack,[3] Emily F. Kerr,[1] Roy G. Gordon,[*,1,2] Michael J. Aziz[*,2]

[1] Department of Chemistry and Chemical Biology, Harvard University, Cambridge, Massachusetts 02138, United States

[2] John A. Paulson School of Engineering and Applied Sciences, Harvard University, Cambridge, Massachusetts 02138, United States

[3] Department of Physics, Harvard University, Cambridge, Massachusetts 02138, United States

[§] These authors contributed equally to this work.

[*] Correspondence: gordon@chemistry.harvard.edu; maziz@harvard.edu

Table of Contents

General information for synthesis and characterization 3

Electrochemical characterization 3

Brief description of electrosynthesis 3

Figure S1. ^{1}H NMR spectra of commercial and synthesized 9,10-dihydroanthracene (DHAC) in DMSO-d_6. 4

Figure S2. ^{1}H NMR spectra of 2,7-, 2,6-DPivOHAC isomers and their mixture (aromatic region) in DMSO-d_6. 5

Figure S3. Photos of undivided cell (a) and divided cell (b). 5

Figure S4. Schematics of (a) undivided cell against the HER and divided cells against (b) the ORR and (c) ferricyanide to ferrocyanide, respectively. 6

Electrosynthesis I. Electrochemical synthesis of DPivOHAQ(COO$^-$) in an undivided cell at 0.1 M concentration, against the hydrogen evolution reaction (HER). 7

Electrosynthesis II. Electrochemical synthesis of DPivOHAQ(COO$^-$) in a divided cell at 0.1 M concentration, against the oxygen reduction reaction (ORR). 8

Electrosynthesis III. Electrochemical synthesis of DPivOHAQ(COO$^-$) in a divided cell at 0.1 M concentration, against the reduction of ferricyanide. 8

Electrosynthesis IV. Electrochemical synthesis of DPivOHAQ(COO$^-$) in a divided cell at 0.5 M concentration with excess hydroxide, against the reduction of ferricyanide. 9

Figure S5. The electrochemical oxidation of 0.5 M DPivOHAC(COO$^-$) (Electrosynthesis IV). ... 10

Figure S6. ^{1}H NMR spectrum of DPivOHAQ in DMSO-d_6 synthesized via the procedure described in Electrosynthesis IV. From the aromatic peak integrations, we found that 89.0% DPivOHAQ was generated (when the two set of peaks at chemical shifts of 7.95 and 8.10 ppm were integrated), 11.0% DPivOHAC was remaining..... 11

Figure S7. Mass spectra of partially electrosynthesized DPivOHAQ (from Electrosynthesis IV) measured by liquid chromatography–mass spectrometry (LC–MS). 12

Scheme S1. Kolbe electrolysis. 13

Electrosynthesis V. Electrochemical synthesis of DPivOHAQ(COO^-) in a divided cell at 0.5 M concentration with a stoichiometric quantity of hydroxide, against the reduction of ferricyanide. 13

Formation of dianthrone during electrosynthesis..... 14

Figure S8. Cell performance of 0.5 M electrosynthesized DPivOHAQ when a stoichiometric quantity of hydroxide was added into the DPivOHAC(COO^-) solution (Electrosynthesis V)..... 14

Figure S9. Voltage profiles of 0.5 M electrosynthesized DPivOHAQ when a stoichiometric quantity of hydroxide was added into the DPivOHAC solution (Electrosynthesis V) with different lower voltage cutoffs [(a) 0.6, (b) 0.2, (c) 0.6, and (d) 0.7 V]..... 15

Figure S10. ^{1}H NMR spectrum of cycled 0.5 M electrosynthesized DPivOHAQ when a stoichiometric quantity of hydroxide was added into the DPivOHAC(COO^-) solution (Electrosynthesis V). 16

Figure S11. LC–MS results of cycled 0.5 M electrosynthesized DPivOHAQ when a stoichiometric quantity of hydroxide was added into the DPivOHAC solution (Electrosynthesis V). 17

Electrosynthesis VI. Electrochemical synthesis of DBAQ(COO^-) in an undivided electrolytic cell at 0.1 M concentration, against the HER. 18

Figure S12. ^{1}H NMR spectra of DBDHAC (bottom), chemically synthesized DBAQ (top), and electrochemically synthesized DBAQ in an undivided cell after varying extents of reaction. 19

Light sensitivity experiments 19

Figure S13. Samples of (a) DPivOHAQ (0.1 M, pH 12) stored for 1 week in the absence of light (– hν) and under a 500 W lamp (+ hν) and of (b) DBAQ (0.1 M, pH 12) stored for 1 week in the absence of light (– hν) and under a 500 W lamp (+ hν). Differences in color were observed between the two samples of each compound. The formation of a film was also observed in the DPivOHAQ sample exposed to light. 20

Figure S14. ^{1}H NMR spectra of samples of DPivOHAQ (0.1 M, pH 12) stored for 1 week in the absence of light (– hν) and under a 500 W lamp (+ hν), each diluted (1:5.5) in pH 14 D_2O (1 M KOD) containing a 9 mM $NaCH_3SO_3$ internal standard (δ 2.6 ppm)..... 21

Figure S15. ^{1}H NMR spectra of samples of DBAQ (0.1 M, pH 12) stored for 1 week in the absence of light (– h*ν*) and under a 500 W lamp (+ h*ν*), each diluted (1:5) in pH 12 D_2O or in DMSO-d_6. 22

Complete synthesis..... 22

Scheme S3. Complete synthetic routes, conditions, and yields of DPivOHAQ and DBAQ when commercially available commodity chemicals are used as starting materials. 23

Figure S16. ^{1}H NMR spectra of commercial and synthesized anthracene (AC) in DMSO-d_6. The peak at 7.37 ppm in the synthesized AC spectrum is from benzene. 23

General information for synthesis and characterization

All reagents were purchased from Sigma-Aldrich or Alfa Aesar and used as received unless otherwise stated. All reactions sensitive to moisture or oxygen were carried out in oven-dried or flame-dried and nitrogen-charged glassware. All anhydrous solvents were saturated with argon and passed through a column of activated alumina immediately prior to use.

^{1}H NMR spectra were recorded on Varian INOVA 500 spectrometers at 500 MHz. NMR spectra were recorded in solutions of deuterated dimethyl sulfoxide (DMSO-d_6) with the residual dimethyl sulfoxide (δ 2.25 ppm for ^{1}H NMR), or deuterated water (D_2O) with the residual H_2O (δ 4.79 ppm for ^{1}H NMR).

LC–MS was conducted on a Bruker microTOF-Q II mass spectrometer. The sample was diluted by water/acetonitrile (V/V = 1:1) to the desired concentration (~20μM) before LC–MS measurements.

Electrochemical characterization

Cyclic voltammetry measurements

Glassy carbon was used as the working electrode for all three-electrode CV tests with a 5 mm diameter glassy carbon working electrode, an Ag/AgCl reference electrode (BASi, pre-soaked in 3 M NaCl solution), and a graphite counter electrode.

All electrochemical oxidation and flow cell cycling was conducted with Biologic equipment and corresponding software.

Flow cell setup

Flow battery experiments were constructed with cell hardware from Fuel Cell Tech (Albuquerque, NM) assembled into a zero-gap flow cell configuration. Pyrosealed POCO graphite flow plates with serpentine flow patterns were used for both electrodes. Each electrode comprised a 5 cm^2 geometric surface area covered by a piece of AvCarb HCBA woven carbon fiber. The membrane is pre-soaked (1 M KOH for 24 hours) Nafion 212.

Brief description of electrosynthesis

Undivided electrolytic cell setup

Working electrode: carbon felt, where **DPivOHAC(COO$^-$)** was oxidized to **DPivOHAQ(COO$^-$)**; counter electrode: carbon rod, where water was reduced to hydrogen gas.

Divided electrolytic cell setup vs. the ORR

Anode: Commercial AvCarb HCBA (woven carbon cloth), where **DPivOHAC(COO$^-$)** was oxidized to **DPivOHAQ(COO$^-$)**; cathode: platinum coated carbon paper (SGL 39AA), where humidified air/oxygen was reduced to hydroxide.

Divided electrolytic cell setup vs. the reduction of ferricyanide

Anode: AvCarb HCBA (woven carbon cloth), where **DPivOHAC(COO⁻)** was oxidized to **DPivOHAQ(COO⁻)**; cathode: AvCarb HCBA (woven carbon cloth), where potassium ferricyanide was reduced to potassium ferrocyanide.

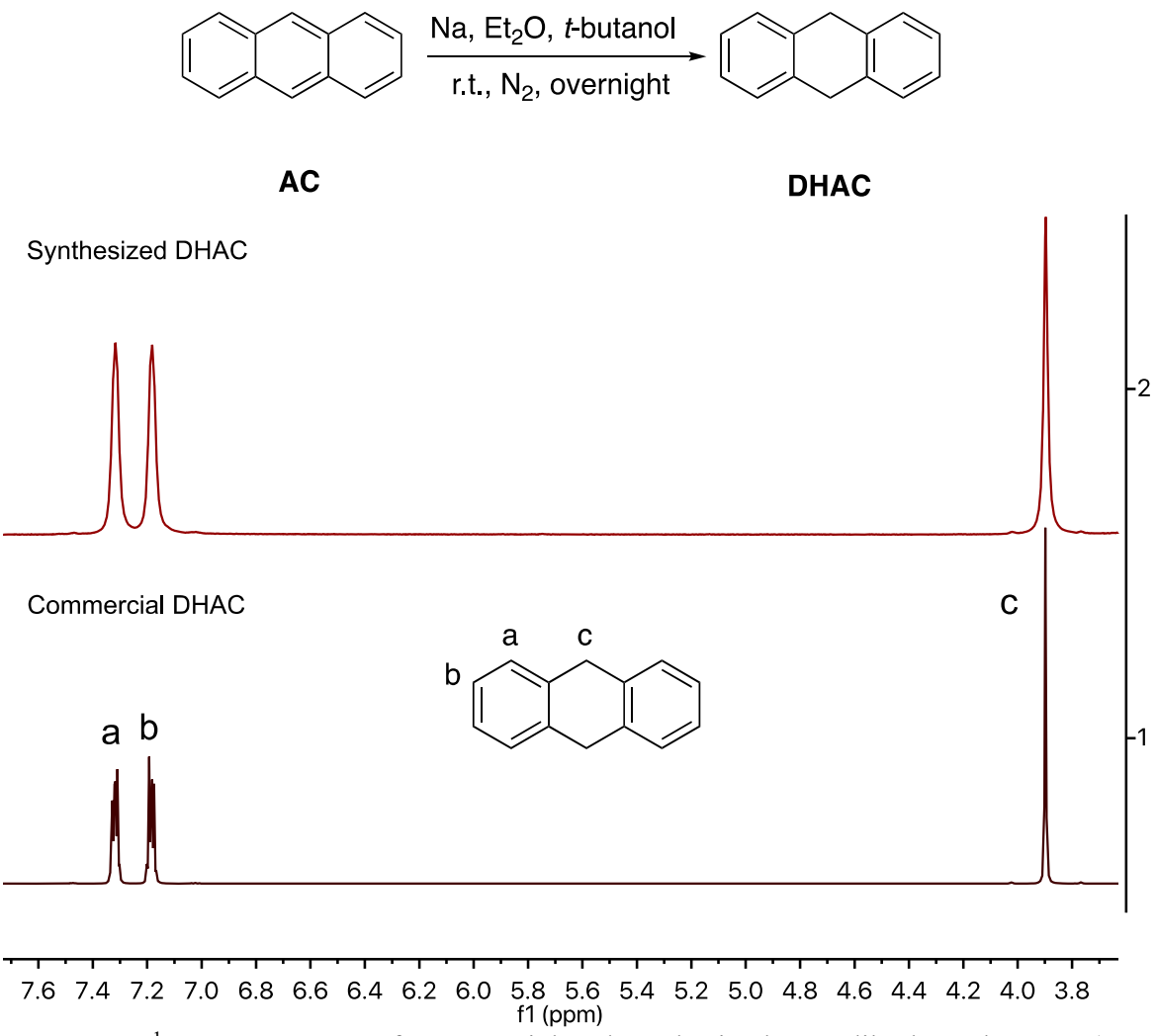

Figure S1. ^{1}H NMR spectra of commercial and synthesized 9,10-dihydroanthracene (**DHAC**) in DMSO-d_6.

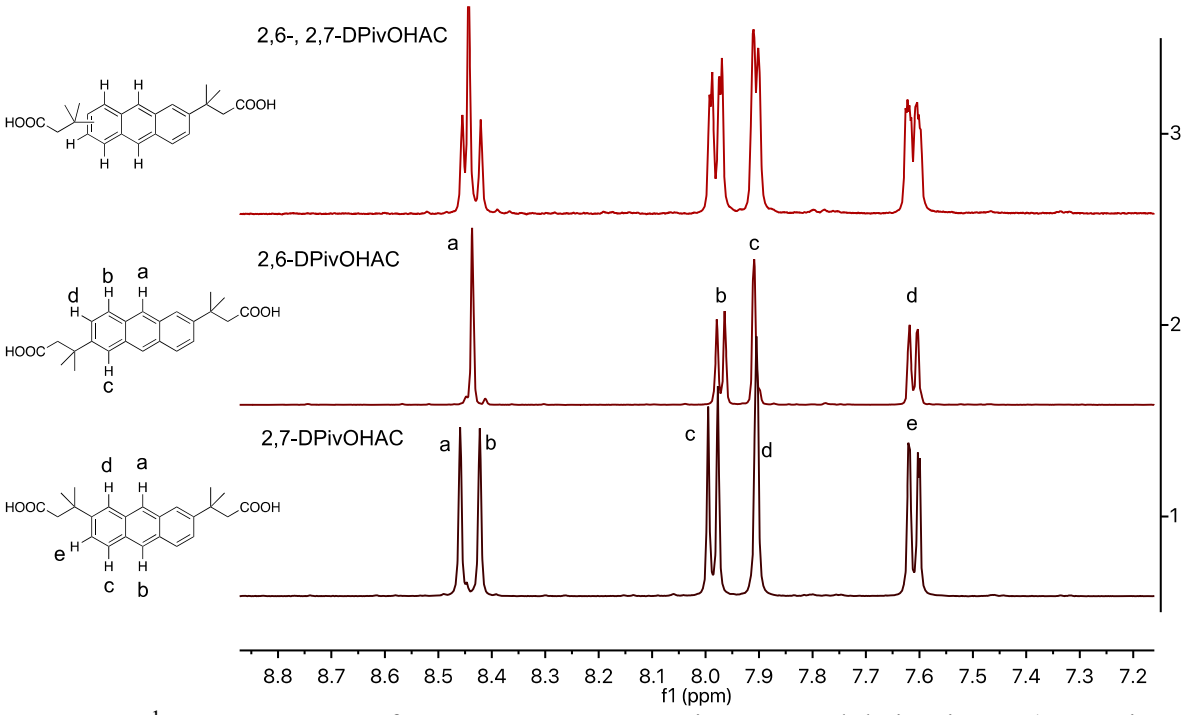

Figure S2. ^{1}H NMR spectra of 2,7-, 2,6-**DPivOHAC** isomers and their mixture (aromatic region) in DMSO-*d*$_6$.

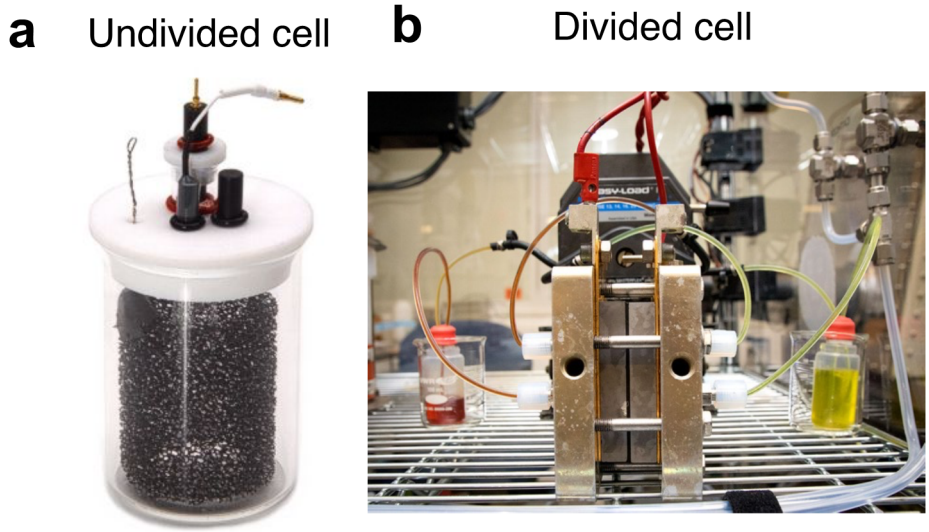

Figure S3. Photos of undivided cell (a) and divided cell (b).

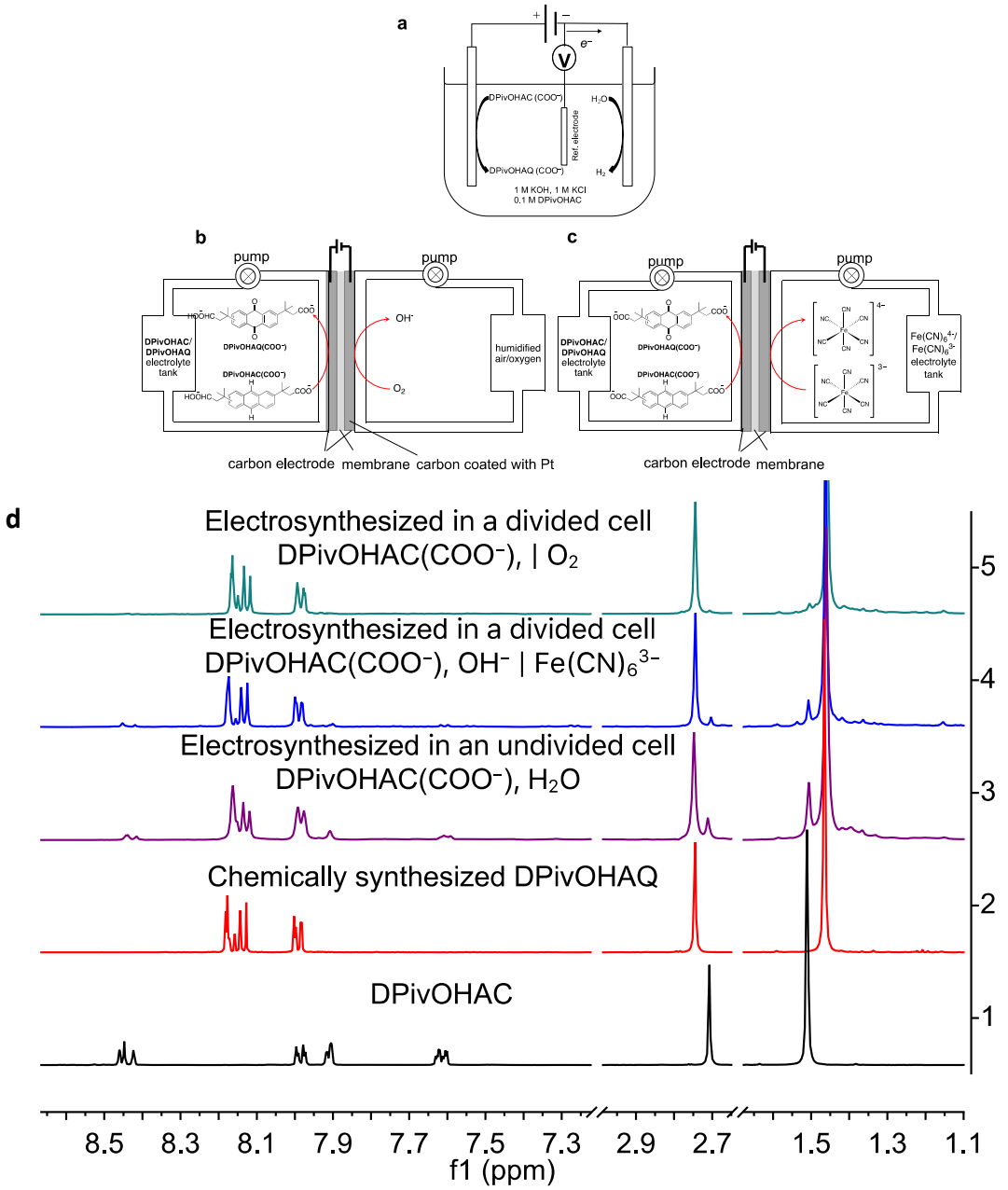

Figure S4. Schematics of (a) undivided cell against the HER and divided cells against (b) the ORR and (c) ferricyanide to ferrocyanide, respectively. (d) ^{1}H NMR spectra of (bottom to top): chemically synthesized **DPivOHAC** (black); chemically synthesized **DPivOHAQ** (red); electrosynthesized **DPivOHAQ** in an undivided cell (purple), 17.3% of **DPivOHAC** remained unreacted according to the integration, yield: 82.7%; electro-synthesized **DPivOHAQ** in a divided cell against $Fe(CN)_6^{3-}$ (blue), 7.0% of **DPivOHAC** remained unreacted according to the integration, yield: 93.0%; electrosynthesized **DPivOHAQ** in a divided cell against O_2 (green), 0 % of **DPivOHAC** remained unreacted according to the integration, yield: 100%. The deuterated solvent is DMSO-*d*$_6$, and the solvent peaks (DMSO and H_2O) were removed to better display the peaks of interest. The electrosynthetic details are described under the headings **Electrosynthesis I, II,** and **III**.

No ion-selective membrane is needed in the undivided cell (against the HER), nor are hydroxides required theoretically because the HER generates the required number of hydroxides for **DPivOHAQ** electrosynthesis. Ideally, the divided cell against the ORR will not require hydroxides either if all generated hydroxides from the ORR can immediately crossover to the **DPivOHAC** anolyte side. The divided cell against ferri- to ferrocyanide reduction needs six equivalents of hydroxide for electrosynthesis, the advantage of which is incorporating the electrosynthesis and flow battery in one setup, and electrosynthesis becomes a part of the on-site setup and takes as long as the energy/power ratio of the battery.

Electrosynthesis I. Electrochemical synthesis of **DPivOHAQ(COO⁻)** in an undivided cell at 0.1 M concentration, against the hydrogen evolution reaction (HER).

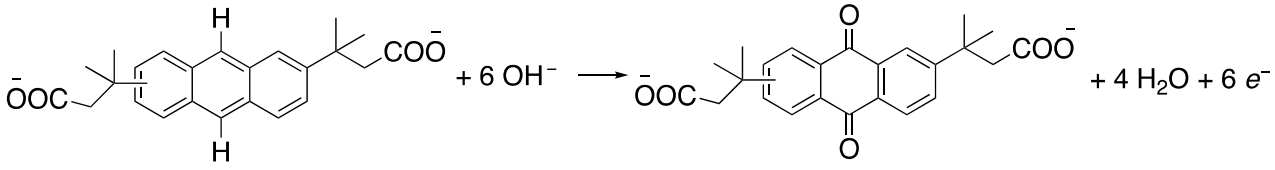

DPivOHAC (COO⁻) DPivOHAQ (COO⁻)

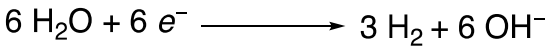

An undivided cell was prepared with carbon felt (XF30A, Toyobo Co., volumetric porosity: 95%) as the working electrode, a carbon rod as the counter electrode, and Ag/AgCl (3 M NaCl) as the reference electrode.

Electrolyte preparation: 0.378 g **DPivOHAC**, 0.745 g KCl, and 0.561 g KOH were dissolved in deionized water to obtain a 10 mL solution containing 0.1 M **DPivOHAC**, 1.0 M KCl, and 1.0 M KOH.

On the working electrode: **DPivOHAC(COO⁻)** was oxidized to **DPivOHAQ(COO⁻)**; on the counter electrode: water was reduced to hydrogen gas.

Electrochemical oxidation of **DPivOHAC(COO⁻)**: while the electrolyte was stirred, a constant potential (1.1 V vs. Ag/AgCl) was applied to the divided electrolytic cell until 120% of the required coulombs were extracted from the working electrode. [0.1 M * 0.01 L * 96485 C/mol * 6 *1.2 = 694.7 C, 6 electrons need to be extracted from every **DPivOHAC** molecule].

Characterization of anolyte: an aliquot (~250 μL) was transferred from the as-prepared anolyte to an Eppendorf® tube (capacity: 1.5 mL) and acidified by a drop of concentrated HCl to obtain **DPivOHAQ** precipitate. The final **DPivOHAQ** precipitate was re-dissolved in DMSO-d_6 for ^{1}H NMR measurement. According to the integration of the ^{1}H NMR spectrum (Figure 3d), the yield is 82.7%. The faradaic efficiency (%) = [yield (%) / 1.2] = 68.9%.

Electrosynthesis II. Electrochemical synthesis of **DPivOHAQ(COO⁻)** in a divided cell at 0.1 M concentration, against the oxygen reduction reaction (ORR).

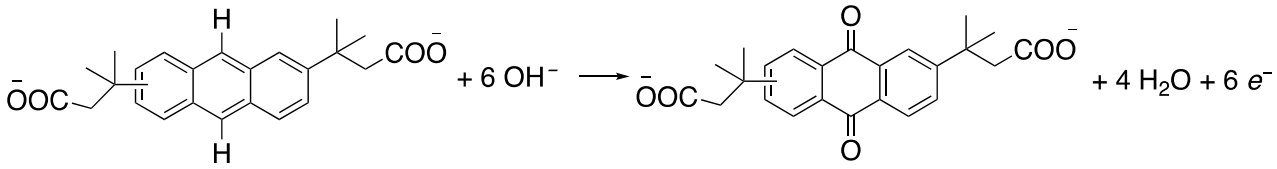

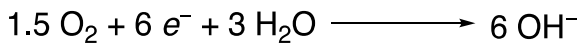

In a flow cell setup (divided electrolytic cell), where unbaked AvCarb HCBA was used on the anode side, the carbon paper was used on the cathode side with coated platinum particles to catalyze the ORR; Nafion® 212 was used as membrane. The high-frequency area specific resistance (HF–ASR) was maintained in the range of 1.48–1.54 Ω cm^2 before and after electrosynthesis.

Anolyte preparation: 0.378 g **DPivOHAC**, 0.745 g KCl, and 0.561 g KOH were dissolved in deionized water to obtain a 10 mL solution containing 0.1 M **DPivOHAC**, 1.0 M KCl, and 1.0 M KOH.

Catholyte preparation: humidified oxygen or air was pumped into the flow cell to participate in the electrochemical reaction.

Electrochemical oxidation of **DPivOHAC(COO⁻)**: a constant voltage (1.8 V) was applied to the divided electrolytic cell until the current decreased to 2 mA/cm^2. The number of extracted electrons was ~1.2 times higher than the theoretical value.

Characterization of anolyte: an aliquot (~250 μL) was transferred from the as-prepared anolyte to an Eppendorf® tube (capacity: 1.5 mL) and acidified by concentrated HCl to obtain **DPivOHAQ** precipitate. The final **DPivOHAQ** precipitate was re-dissolved in DMSO-d_6 for ^{1}H NMR measurement. According to the integration of the ^{1}H NMR spectrum (Figure 3d), the yield is 100%. The faradaic efficiency (%) = [yield (%) / 1.2] = 83.3%.

Electrosynthesis III. Electrochemical synthesis of **DPivOHAQ(COO⁻)** in a divided cell at 0.1 M concentration, against the reduction of ferricyanide.

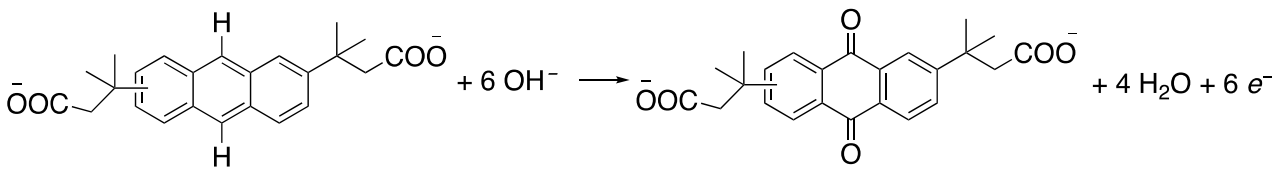

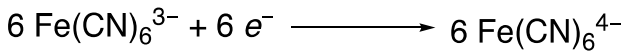

In a flow cell setup (divided electrolytic cell), unbaked AvCarb HCBA (woven carbon cloth) was used as electrodes for both sides; Nafion® 212 was used as the membrane. The high-frequency area specific resistance (HF−ASR) was maintained at ~1.12 Ω cm^2 before and after electrosynthesis.

Anolyte preparation: 0.378 g **DPivOHAC**, 0.745 g KCl, and 0.561 g KOH were dissolved in deionized water to obtain a 10 mL solution containing 0.1 M **DPivOHAC**, 1.0 M KCl, and 1.0 M KOH.

Catholyte preparation: 3.292 g $K_3Fe(CN)_6$, 7.445 g KCl, and 2.805 g KOH were dissolved in deionized water to obtain a 100 mL solution containing 0.1 M $K_3Fe(CN)_6$, 1.0 M KCl, and 0.5 M KOH.

The reason for which 0.5 M KOH was added to the catholyte is to counterbalance the added OH^- in the anolyte, which is required for the electrosynthesis, thereby suppressing the loss of OH^- from the anolyte to the catholyte due to crossover.

Electrochemical oxidation of **DPivOHAC(COO$^-$)**: a constant current density (20 mA/cm^2) was applied to the divided cell for at most 1.5 hours with a 1.2 V voltage cutoff; when either time or voltage reached the limit, the potential was held (1.2 V vs. ferro-/ferricyanide) until the current decreased to 2 mA/cm^2. The number of extracted electrons was ~1.2 times higher than the theoretical value.

Characterization of anolyte: an aliquot (~250 μL) was transferred from the as-prepared anolyte to an Eppendorf® tube (capacity: 1.5 mL) and acidified by a drop of concentrated HCl to obtain **DPivOHAQ** precipitate. The final **DPivOHAQ** precipitate was re-dissolved in DMSO-d_6 for ^{1}H NMR measurement. According to the integration of the ^{1}H NMR spectrum (Figure 3d), the yield is 93.0%. The faradaic efficiency (%) = [yield (%) / 1.2] = 77.5%.

Because a few aliquots were transferred and the volume of as-prepared **DPivOHAQ** changed, 5 mL of the **DPivOHAQ** solution was used as the negolyte and 100 mL of the ferro-/ferricyanide solution [~0.06 M $K_4Fe(CN)_6$ and ~0.04 M $K_3Fe(CN)_6$] generated from **Electrosynthesis III** was used as the posolyte for charge–discharge cycling. Due to leakage, 4.5 mL of **DPivOHAQ** remained for subsequent cycling.

Electrosynthesis IV. Electrochemical synthesis of **DPivOHAQ(COO$^-$)** in a divided cell at 0.5 M concentration with excess hydroxide, against the reduction of ferricyanide.

In a flow cell setup (divided electrolytic cell), unbaked AvCarb HCBA (woven carbon cloth) was used as electrodes for both sides; Nafion® 212 was used as the membrane. The high-frequency area specific resistance (HF−ASR) was maintained at ~1.1 Ω cm^2 before and after electrosynthesis.

Anolyte preparation: 1.89 g **DPivOHAC**, 0.745 g KCl, and 0.567 g KOH were dissolved in deionized water to obtain a 10 mL solution containing 0.5 M **DPivOHAC**, 1.0 M KCl, and 1.0 M KOH. Although the **DPivOHAC** electrochemical oxidation requires OH^- ions, we observed that

0.5 M **DPivOHAC** tends to crash out of solution when the concentration of KOH exceeds 1.5 M. To circumvent this precipitation issue, we added 1.5 times the required amount of KOH pellets (2.52 g) (*i.e.*, 1.5 times 6 equivalents relative to **DPivOHAC**) into the anolyte over the course of constant current charging. According to the Nernst equation, the cell voltage is a function of [OH^-]; thus, the voltage fluctuation reflects the addition of KOH in Figure S5.

Catholyte preparation: 16.46 g $K_3Fe(CN)_6$, 7.445 g KCl, and 2.805 g KOH were dissolved in deionized water to obtain a 100 mL solution containing 0.5 M $K_3Fe(CN)_6$, 1.0 M KCl, and 0.5 M KOH.

Electrochemical oxidation of **DPivOHAC(COO^-)**: a constant current density (100 mA/cm^2) was applied to the divided cell for at most 1.7 hours with a 1.2 V voltage cutoff; when either time or voltage reached the limit, the potential was held (1.2 V vs. ferro-/ferricyanide) until the current decreased to 12 mA/cm^2. The number of extracted electrons was ~1.2 times higher than the theoretical value.

Characterization of anolyte: an aliquot (~250 μL) was transferred from the as-prepared anolyte to an Eppendorf® tube (capacity: 1.5 mL) and acidified by a drop of concentrated HCl to obtain **DPivOHAQ** precipitate. The final **DPivOHAQ** precipitate was re-dissolved in DMSO-d_6 for ^1H NMR measurement; the yield is 89.0%. The faradaic efficiency (%) = [yield (%) / 1.2] = 74.2%.

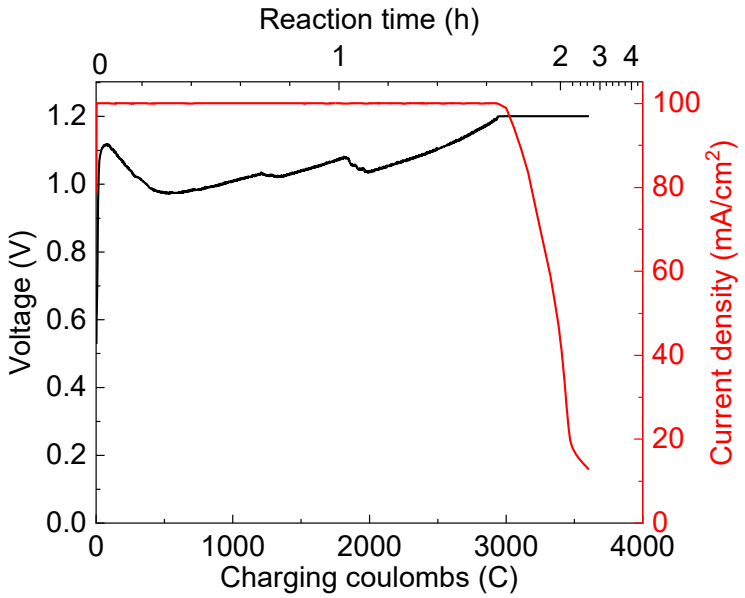

Figure S5. The electrochemical oxidation of 0.5 M **DPivOHAC(COO^-)** (**Electrosynthesis IV**).

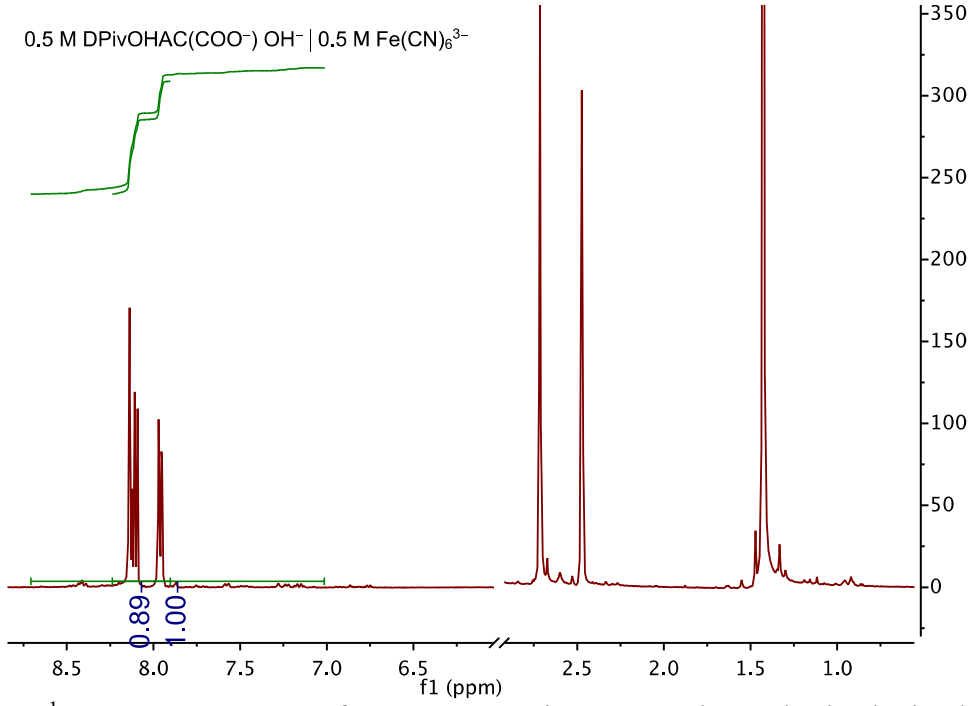

Figure S6. ^{1}H NMR spectrum of **DPivOHAQ** in DMSO-d_6 synthesized via the procedure described in **Electrosynthesis IV**. From the aromatic peak integrations, we found that 89.0% **DPivOHAQ** was generated (when the two set of peaks at chemical shifts of 7.95 and 8.10 ppm were integrated), 11.0% **DPivOHAC** was remaining.

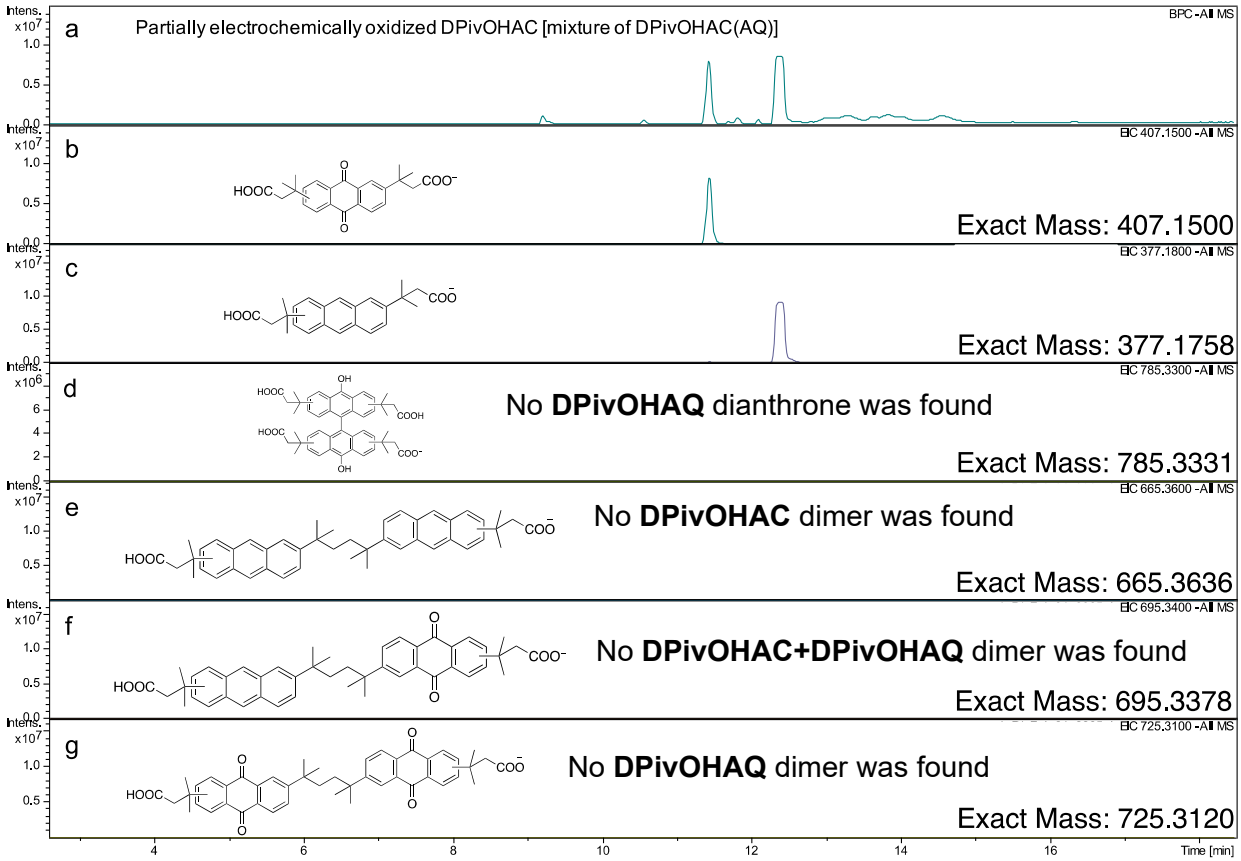

Figure S7. Mass spectra of partially electrosynthesized **DPivOHAQ** (from **Electrosynthesis IV**) measured by liquid chromatography–mass spectrometry (LC–MS). (a) The peak intensity and retention time of partially electrosynthesized **DPivOHAQ** under negative mode. (b) The peak intensity and retention time of **DPivOHAQ** under negative mode. (c) The peak intensity and retention time of **DPivOHAC** under negative mode. (d) The peak intensity and retention time of the **DPivOHAQ** dianthrone under negative mode. No peak was found in the given retention time region, which, in combination with the absence of impurities in the ^{1}H NMR spectra in Figures 3d and S6, indicates that no observable **DPivOHAQ** dianthrone was generated during the electrosynthesis. (e)-(f) The peak intensity and retention time of **DPivOHAQ(AC)**-related Kolbe electrolysis byproducts under negative mode. No peak was found in the given retention time region, which, in combination with the absence of impurities in the ^{1}H NMR spectra in Figures 3d and S6, indicates that no observable **DPivOHAQ(AC)**-related Kolbe electrolysis byproducts were generated during the electrosynthesis.

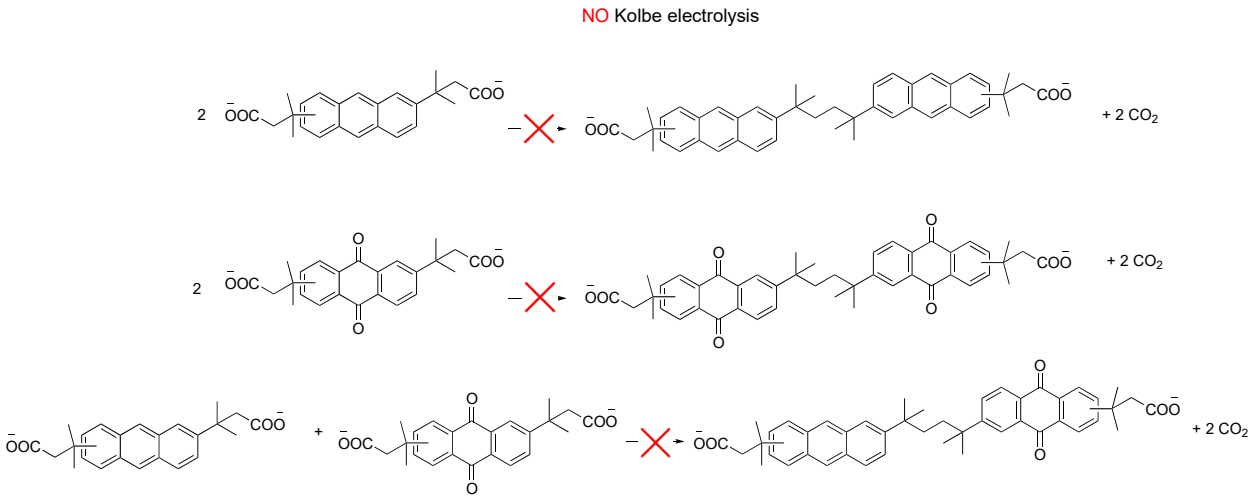

Scheme S1. Kolbe electrolysis. Kolbe electrolysis-related byproducts are not expected in our cell, as the decarboxylation and dimerization reactions usually require much higher voltages and precious-metal-based electrodes.[S1] In our cell, we use carbon electrodes and an applied potential of 1.2 V. Additionally, we did not detect any dimer formation from LC–MS measurements.

Electrosynthesis V. Electrochemical synthesis of **DPivOHAQ(COO⁻)** in a divided cell at 0.5 M concentration with a stoichiometric quantity of hydroxide, against the reduction of ferricyanide.

In a flow cell setup (divided electrolytic cell), unbaked AvCarb HCBA (woven carbon cloth) was used as electrodes for both sides; Nafion® 212 was used as the membrane. The high-frequency area specific resistance (HF–ASR) was maintained at ~1.45 Ω cm^2 before and after electrosynthesis.

Anolyte preparation: 1.89 g **DPivOHAC**, 0.745 g KCl, and 0.567 g KOH were dissolved in deionized water to obtain a 10 mL solution containing 0.5 M **DPivOHAC**, 1.0 M KCl, and 1.01 M KOH. We added the stoichiometric quantity of KOH pellets (1.68 g) (*i.e.*, 6 equivalents relative to **DPivOHAC**) into the anolyte over the course of constant current charging.

Catholyte preparation: 16.46 g $K_3Fe(CN)_6$, 7.445 g KCl, and 2.805 g KOH were dissolved in deionized water to obtain a 100 mL solution containing 0.5 M $K_3Fe(CN)_6$, 1.0 M KCl, and 0.5 M KOH.

Electrochemical oxidation of **DPivOHAC(COO⁻)**: a constant current density (100 mA/cm^2) was applied to the divided electrolytic cell for at most 1.7 hours with a 1.2 V voltage cutoff; when either time or voltage reached the limit, the potential was held (1.2 V vs. ferro-/ferricyanide) until the current decreased to 12 mA/cm^2. The number of extracted electrons was ~1.2 times higher than the theoretical value.

Characterization of anolyte: an aliquot (~250 μL) was transferred from the as-prepared anolyte to an Eppendorf® tube (capacity: 1.5 mL) and acidified by a drop of concentrated HCl to obtain **DPivOHAQ** precipitate. The final **DPivOHAQ** precipitate was re-dissolved in DMSO-d_6 for ^{1}H NMR measurement; the yield is 81.8%. The faradaic efficiency (%) = [yield (%) / 1.2] = 68.2%.

Formation of dianthrone during electrosynthesis

Anthrone dimers can be produced during the electrosynthesis when insufficient hydroxide is present.

When there is excess hydroxide in the solution, although some OH^- ions will be electrochemically oxidized to oxygen via the OER, the remaining OH^- ions are sufficient for the conversion of $\mathbf{A}^-$ to $\mathbf{AQ}^{2-}$.

When there is no excess hydroxide, given that the OER side reaction is an inevitable competing reaction, there will be insufficient OH^- ions for the conversion of $\mathbf{A}^-$ to $\mathbf{AQ}^{2-}$; instead, the anthrone anion $\mathbf{A}^-$ may be oxidatively dimerized to the dianthrone **DA**. The following figures and scheme illustrate how **DA** was identified and propose its corresponding electrochemistry.

During the electrochemical oxidation of the 10 mL 0.5 M **DPivOHAC(COO$^-$)** at pH 12, only 1.68 g of KOH (10*0.001 L*0.5 M*6*56.1056 g/mol =1.68 g) were added to the solution. Although there is some additional KOH added to the potassium ferricyanide side, hydroxide cannot cross over to the **DPivOHAC** side of the cell sufficiently rapidly to offset its consumption by **DPivOHAC** oxidation and the OER.

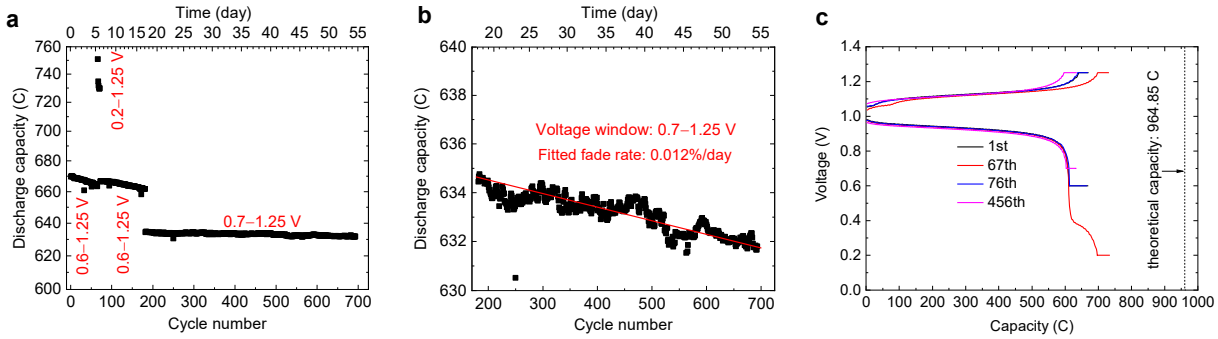

Figure S8. Cell performance of 0.5 M electrosynthesized **DPivOHAQ** when a stoichiometric quantity of hydroxide was added into the **DPivOHAC(COO$^-$)** solution (**Electrosynthesis V**). (a) The long-term cycling performance with adjusted lower voltage cutoffs. (b) The zoomed in discharge capacity when 0.7–1.25 V voltage cutoffs were applied; the fitted temporal fade rate was 0.01%/day. (c) The voltage profiles at varying cycle numbers with different lower voltage cutoffs.

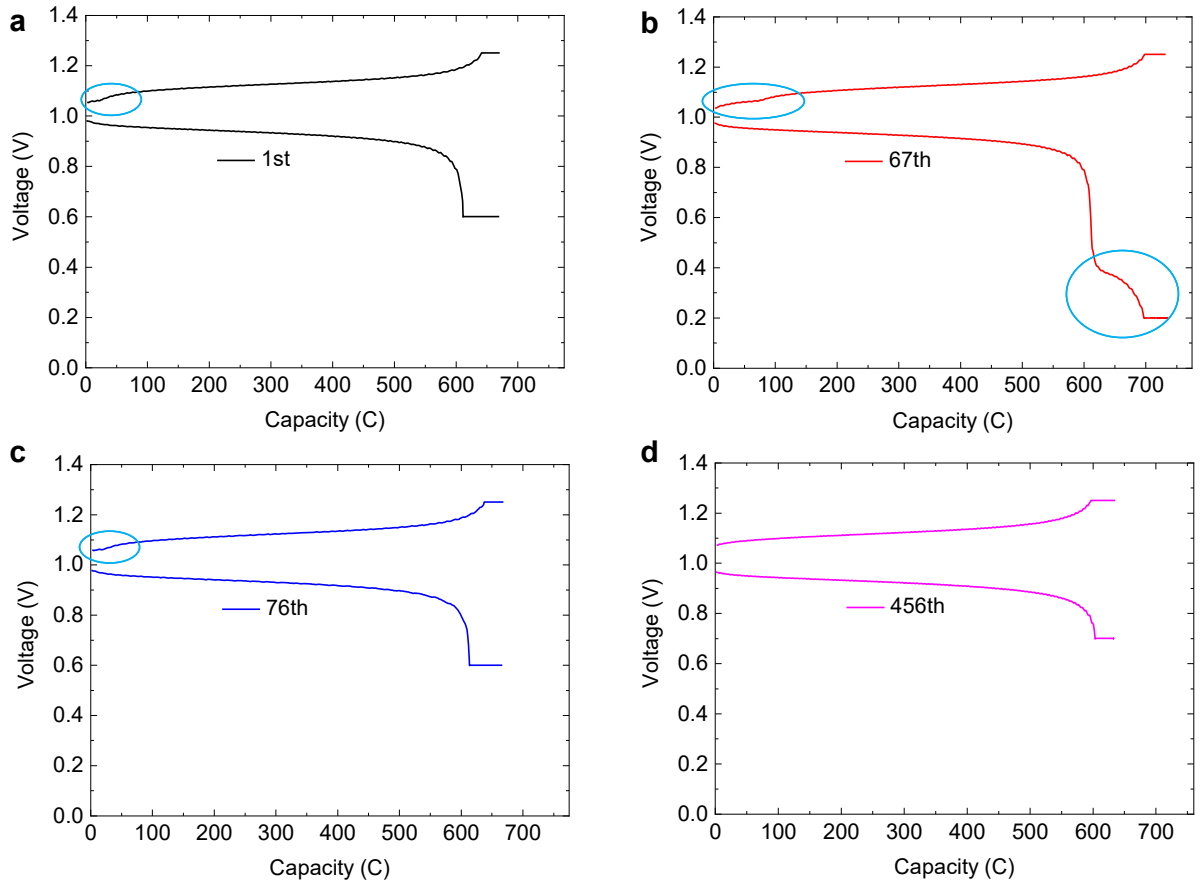

Figure S9. Voltage profiles of 0.5 M electrosynthesized **DPivOHAQ** when a stoichiometric quantity of hydroxide was added into the **DPivOHAC** solution (**Electrosynthesis V**) with different lower voltage cutoffs [(a) 0.6, (b) 0.2, (c) 0.6, and (d) 0.7 V]. The upper voltage cutoff is kept constant at 1.25 V for the duration of cell cycling.

In the 1st cycle, the region in (a) circled in cyan shows a small plateau, indicating some redox-active byproducts were produced during the electrosynthesis. In the 67th cycle, after lowering the lower cutoff from 0.6 to 0.2 V, we can clearly see the discharge plateau (in the region of 0.2–0.4 V) attributed to byproducts, and the charge plateau attributed to byproducts is also becoming longer. In the 76th cycle, after elevating the lower cutoff back to 0.6 V, the shape of the charge profile becomes nearly the same as the one in the 1st cycle. After the lower voltage cutoff was further increased to 0.7 V, in the 456th cycle, the small plateau attributed to the byproducts disappeared.

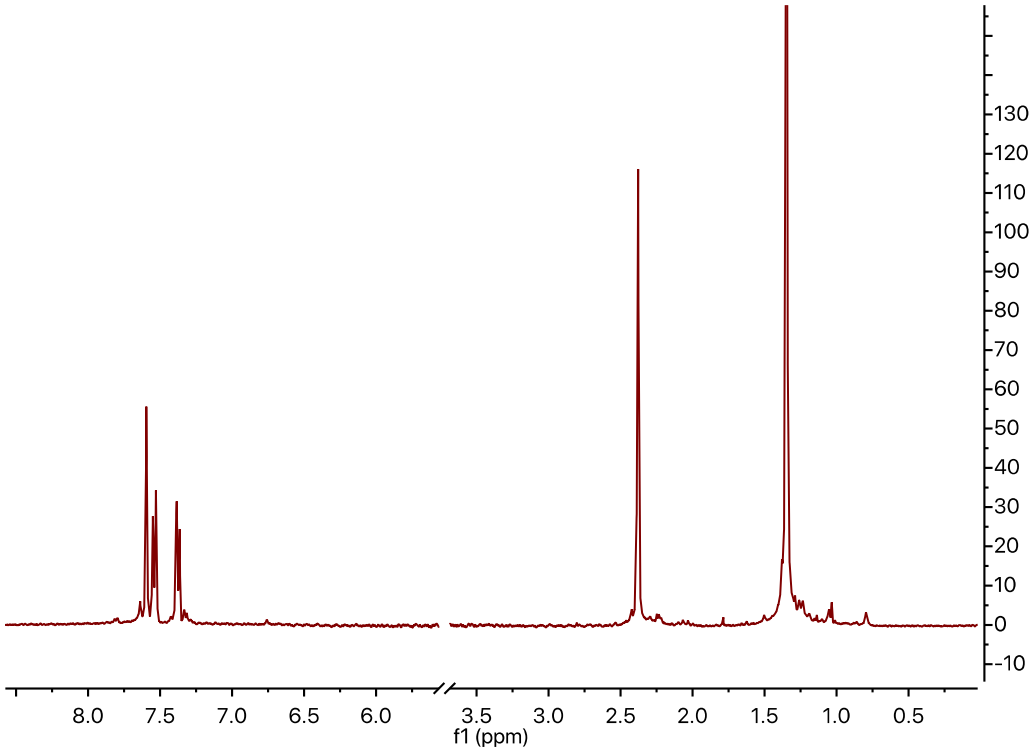

Figure S10. ^{1}H NMR spectrum of cycled 0.5 M electrosynthesized **DPivOHAQ** when a stoichiometric quantity of hydroxide was added into the **DPivOHAC(COO^{-})** solution (**Electrosynthesis V**). The solvent peak was removed to clearly show both aromatic and aliphatic regions of the cycled **DPivOHAQ** solution. The deuterated solvent is D_2O. The dominating peaks can be assigned to **DPivOHAQ**. Some small impurity peaks were observed, but they are difficult to identify. The percentages of side products are very close to the detection limit of the ^{1}H NMR instrument.

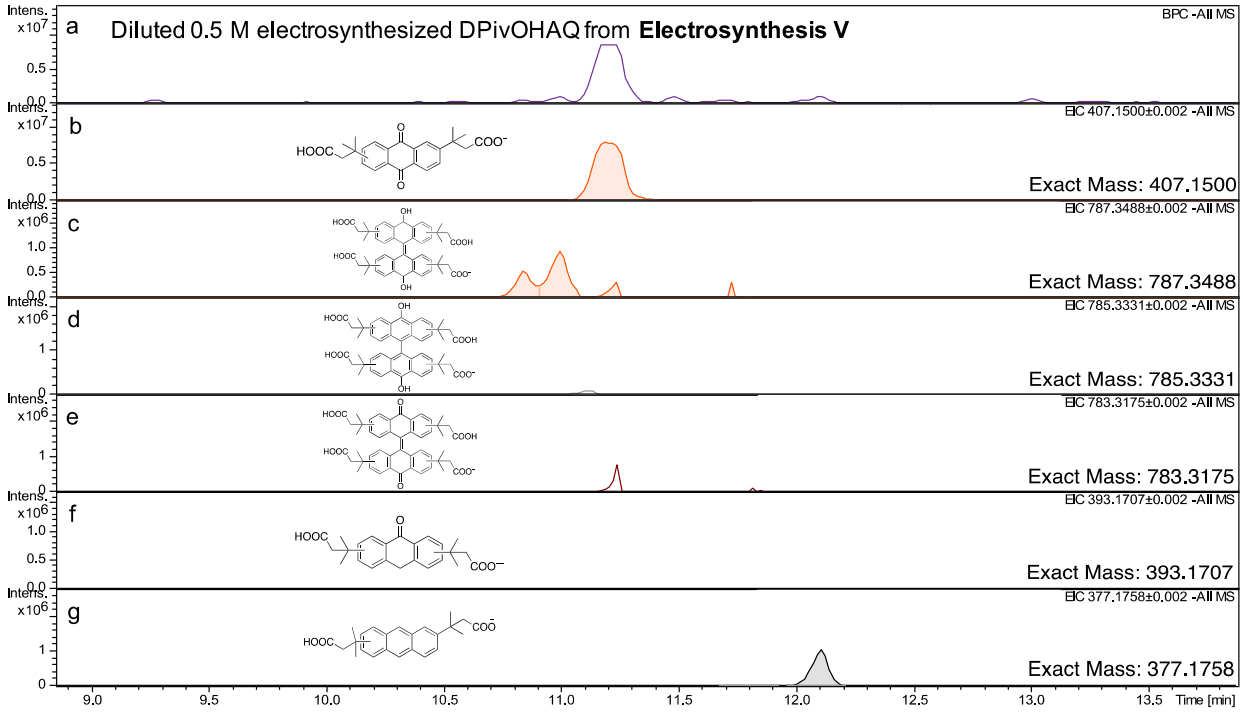

Figure S11. LC–MS results of cycled 0.5 M electrosynthesized **DPivOHAQ** when a stoichiometric quantity of hydroxide was added into the **DPivOHAC** solution (**Electrosynthesis V**). (a) The base peak chromatogram of the sample, showing all peaks observed by mass spectrometry under negative mode. (b) The peak intensity and retention time of **DPivOHAQ–1H** under negative mode. (c) The peak intensity and retention time of **dianthrone+1H** under negative mode. (d) The peak intensity and retention time of **dianthrone–1H** under negative mode. (e) The peak intensity and retention time of **dianthrone–3H** under negative mode. (f) The peak intensity and retention time of **anthrone–1H** under negative mode (none observed). (g) The peak intensity and retention time of **DPivOHAC–1H** under negative mode. By integrating the peak areas in (b), (c), (d), (e), (f) and (g), we found the percentages of **DPivOHAQ** (81.8%), **dianthrone+1H** (10.2%), **dianthrone–1H** (0.4%), **dianthrone–3H** (1.3%), and **DPivOHAC** (6.3%).

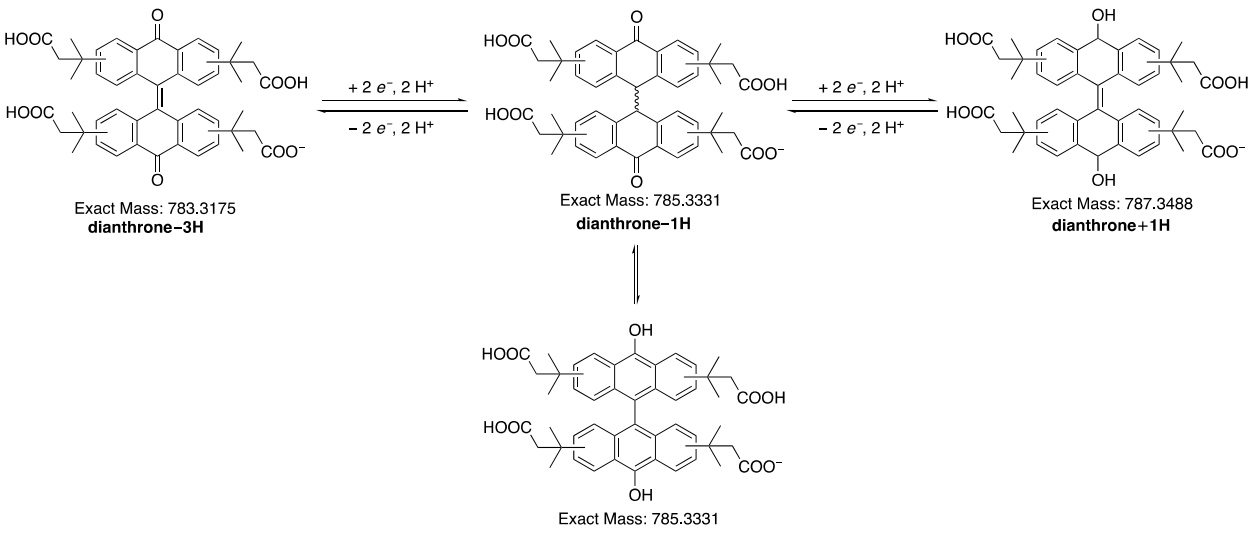

Scheme S2. Proposed possible redox reactions of dianthrones. Because the **dianthrone+1H** (exact mass: 787.3488) and **dianthrone–3H** (exact mass: 783.3175) were detected and plateaus were observed from the voltage profiles, we propose that there are three redox-active states for the dianthrones.

Electrosynthesis VI. Electrochemical synthesis of **DBAQ(COO⁻)** in an undivided electrolytic cell at 0.1 M concentration, against the HER.

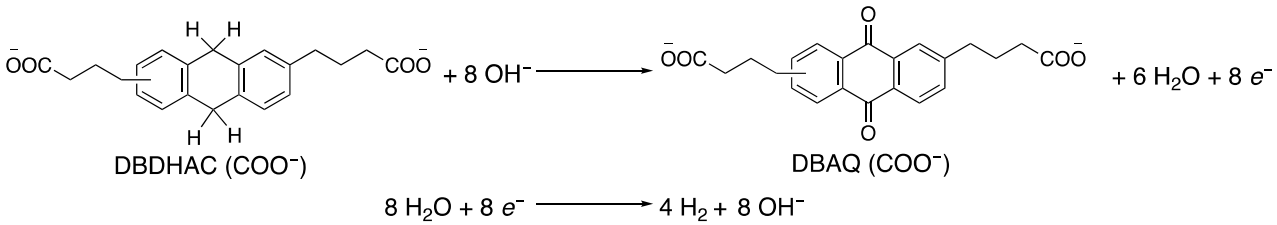

An undivided electrolytic cell was prepared with carbon felt (XF30A, Toyobo Co., volumetric porosity: 95%) as the working electrode, a carbon rod as the counter electrode, and Ag/AgCl (3 M NaCl) as the reference electrode.

Electrolyte preparation: 0.35 g **DBDHAC** (synthesized by following our previous work), 0.745 g KCl, and 0.561 g KOH were dissolved in deionized water to obtain a 10 mL solution containing 0.1 M **DBDHAC**, 1.0 M KCl, and 1.0 M KOH.

On the working electrode: **DBDHAC** was oxidized to **DBAQ**; on the counter electrode: water was reduced to hydrogen gas.

Electrochemical oxidation of **DBDHAC(COO⁻)**: while the electrolyte was stirring, a constant potential (1.1 V vs. Ag/AgCl) was applied to the divided electrolytic cell until 120% of the required coulombs were extracted from the working electrode. [0.1 M * 0.01 L * 96485 C/mol * 8 * 1.2 = 926.3 C; 8 electrons need to be extracted from every **DBDHAC** molecule].

Characterization of anolyte: an aliquot (250 µL) was transferred from the as-prepared anolyte to an Eppendorf® tube (capacity: 1.5 mL) and acidified by a drop of concentrated HCl to obtain **DBAQ** precipitate. The final **DBAQ** precipitate was re-dissolved in DMSO-d_6 for ^{1}H NMR measurement. According to the integration of the ^{1}H NMR spectrum in the Figure S12, the yield is 70%. The faradaic efficiency (%) = [yield (%) / 1.2] = 58.3%.

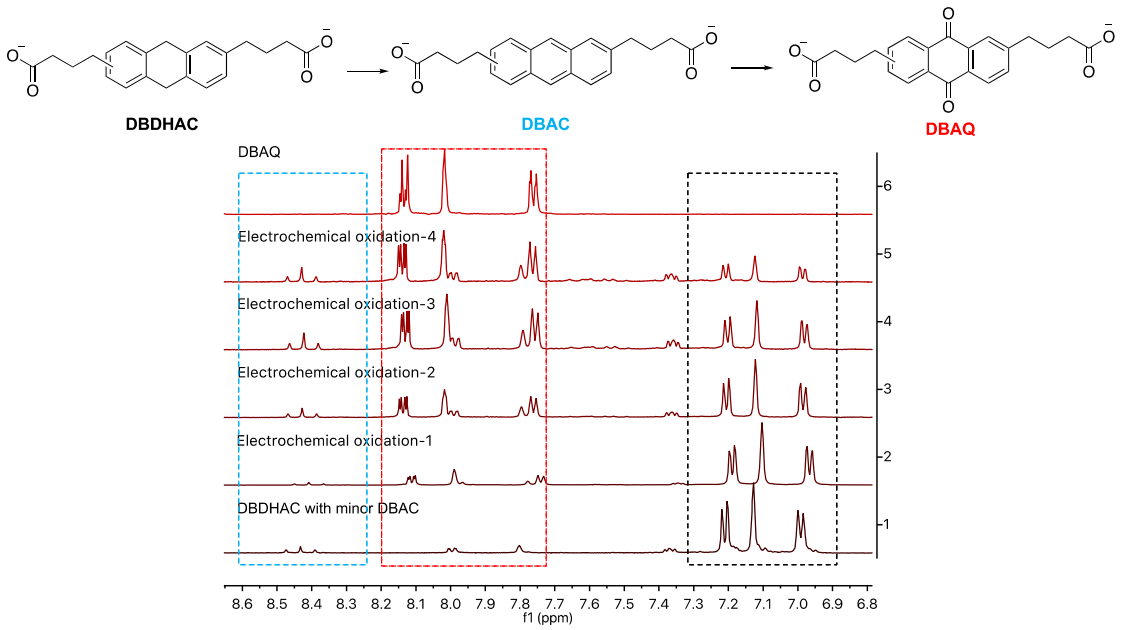

Figure S12. ^{1}H NMR spectra of **DBDHAC** (bottom), chemically synthesized **DBAQ** (top), and electrochemically synthesized **DBAQ** in an undivided cell after varying extents of reaction. **DBDHAC**: 4,4'-(9,10-dihydroanthracene-diyl)dibutanoic acid; **DBAC:** 4,4'-(anthracene-diyl)dibutanoic acid; **DBAQ:** 4,4'-(9,10-anthraquinone-diyl)dibutanoic acid. The time interval between successive measurements labeled electrochemical oxidation-1, 2, 3, and 4 is approximately one hour. The deuterated solvent is DMSO-d_6.

Light sensitivity experiments

It has been reported that quinones and related compounds can decompose in the presence of light.[S2-S6] In order to determine the light sensitivity of **DPivOHAQ** and **DBAQ**, we compared solutions of each compound held in the presence of and in the absence of light for 1 week. Two samples of **DPivOHAQ** (0.1 M, pH 12 in water with 1 M KCl, 1.5 mL each) and two samples of **DBAQ** (0.1 M, pH 12 in water, 1.5 mL each) were prepared in separate FEP bottles (VWR Catalog No. 16071-008). For each compound, one sample was wrapped in aluminum foil and stored in a dark drawer for 1 week. The other sample was held for 1 week under a quartz halogen lamp with a controllable output of 50–1000 W set to 500 W (CowboyStudio QL-1000 W HEAD; ePhotoInc QL 1000Bulb). The samples exposed to light were allowed to float at the top of a water bath containing approximately 16 L of water to dissipate excess heat produced by the lamp (the liquid level decreased gradually due to evaporation and was replenished daily). The liquid level was maintained at a distance of approximately 20 cm from the light source.

After 1 week, differences in color were observed between the samples of each compound stored in the dark and exposed to light (Figure S13). The formation of a film was also observed in the

DPivOHAQ sample exposed to light. ^{1}H NMR spectra of each sample demonstrate decomposition of both compounds stored in the presence of light (Figures S14 and S15).

We therefore wrapped the electrolyte reservoirs with aluminum foil to avoid decomposition due to light exposure during cell cycling.

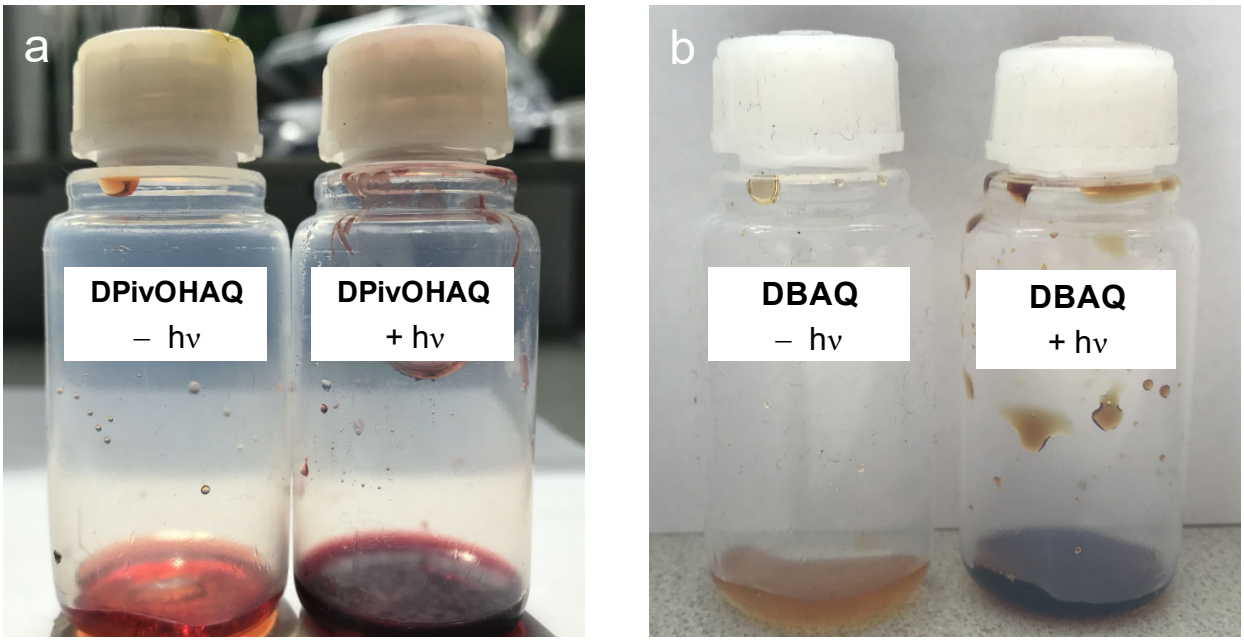

Figure S13. Samples of (a) **DPivOHAQ** (0.1 M, pH 12) stored for 1 week in the absence of light (– hν) and under a 500 W lamp (+ hν) and of (b) **DBAQ** (0.1 M, pH 12) stored for 1 week in the absence of light (– hν) and under a 500 W lamp (+ hν). Differences in color were observed between the two samples of each compound. The formation of a film was also observed in the **DPivOHAQ** sample exposed to light.

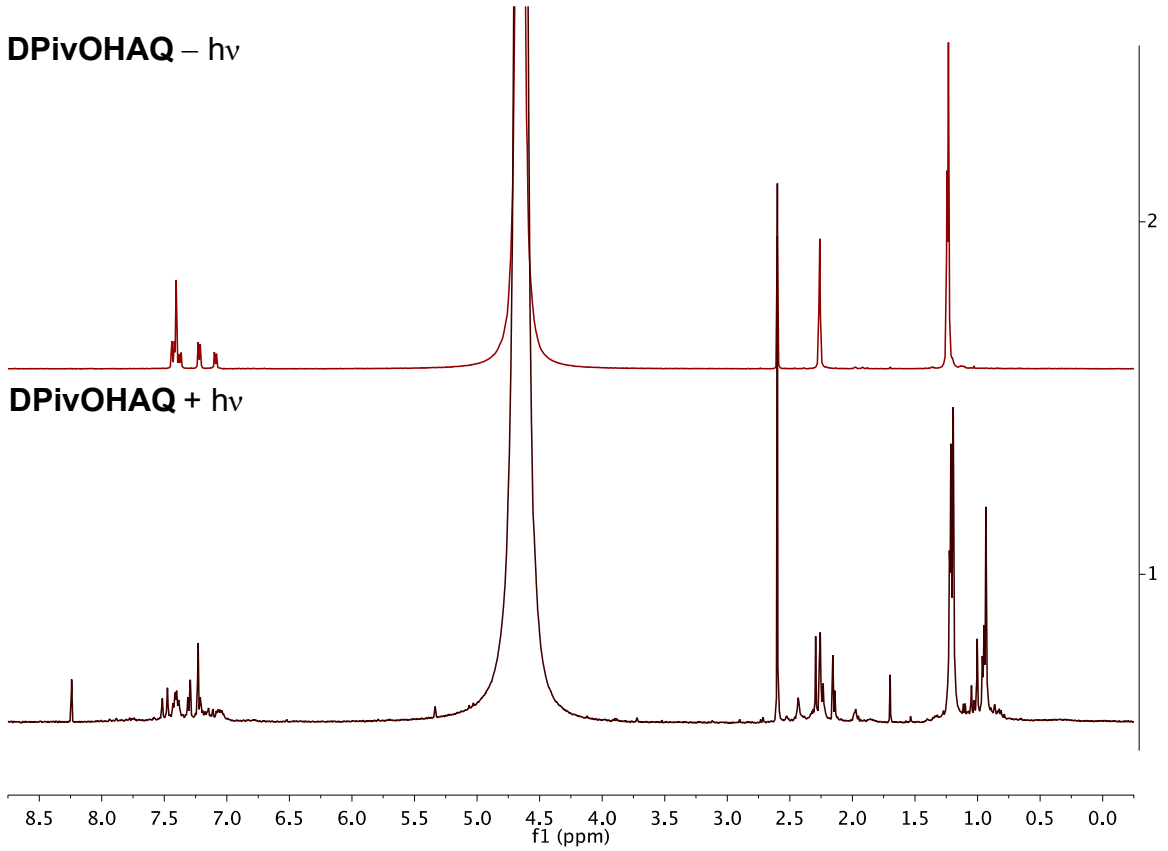

Figure S14. ^{1}H NMR spectra of samples of **DPivOHAQ** (0.1 M, pH 12) stored for 1 week in the absence of light (– hν) and under a 500 W lamp (+ hν), each diluted (1:5.5) in pH 14 D_2O (1 M KOD) containing a 9 mM $NaCH_3SO_3$ internal standard (δ 2.6 ppm).

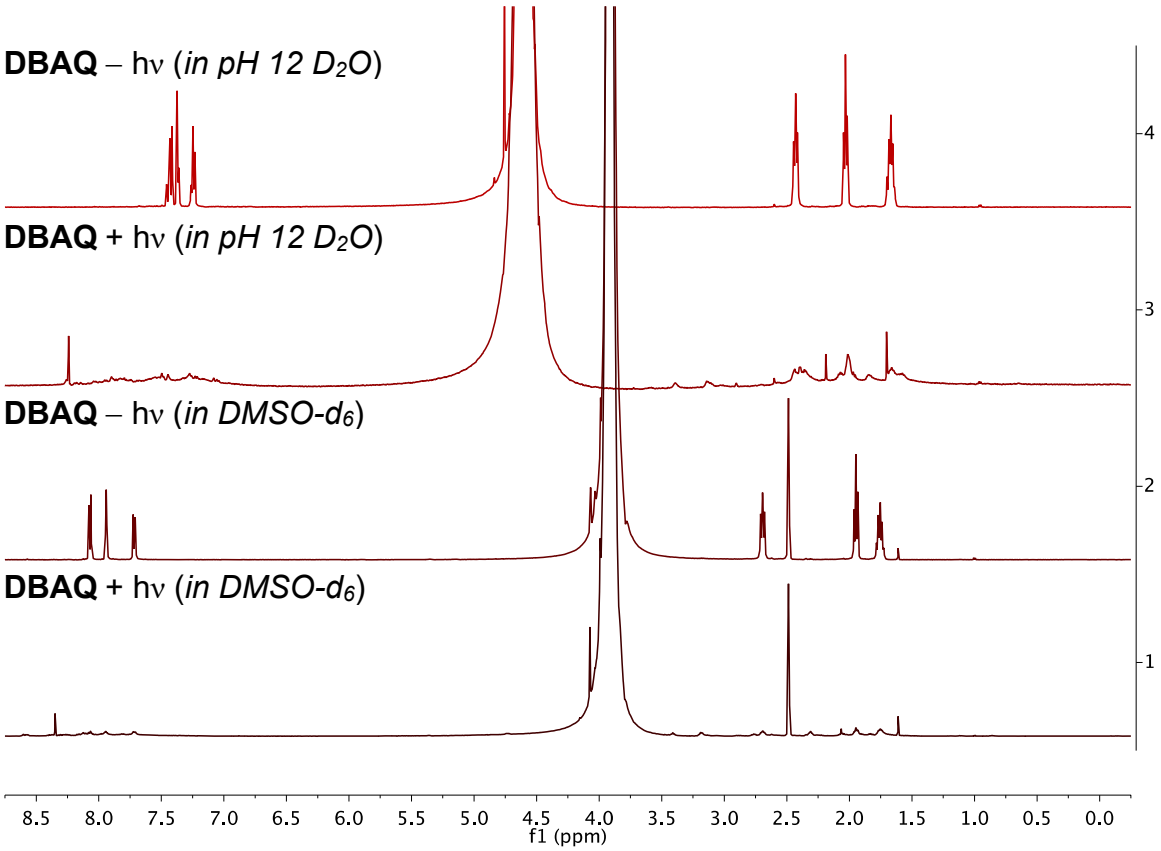

Figure S15. ^{1}H NMR spectra of samples of **DBAQ** (0.1 M, pH 12) stored for 1 week in the absence of light (– hν) and under a 500 W lamp (+ hν), each diluted (1:5) in pH 12 D_2O or in DMSO-d_6.

Complete synthesis

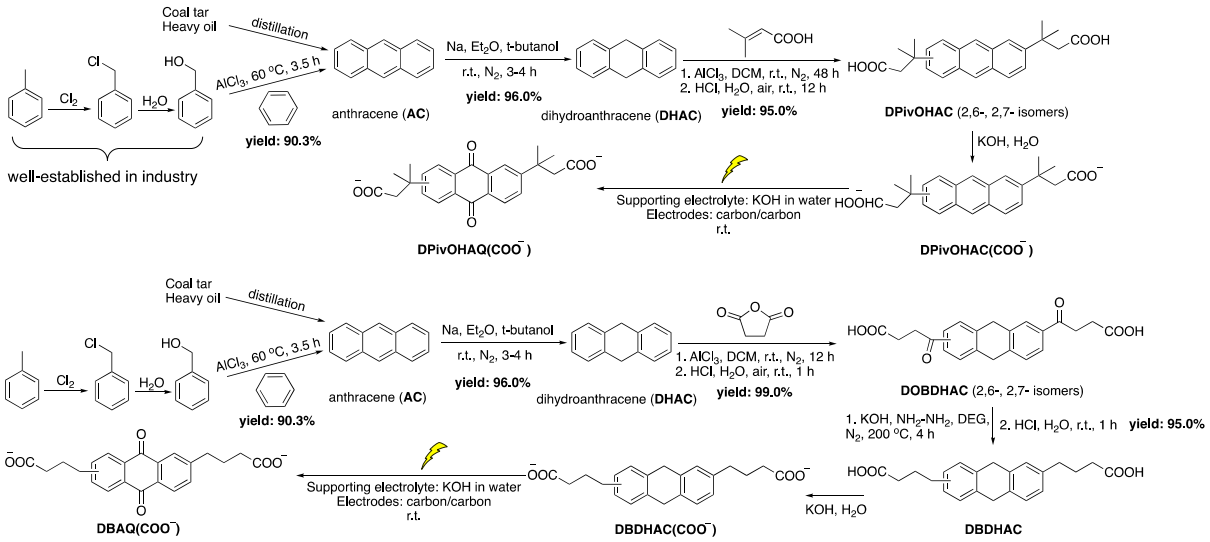

Scheme S3. Complete synthetic routes, conditions, and yields of **DPivOHAQ** and **DBAQ** when commercially available commodity chemicals are used as starting materials.

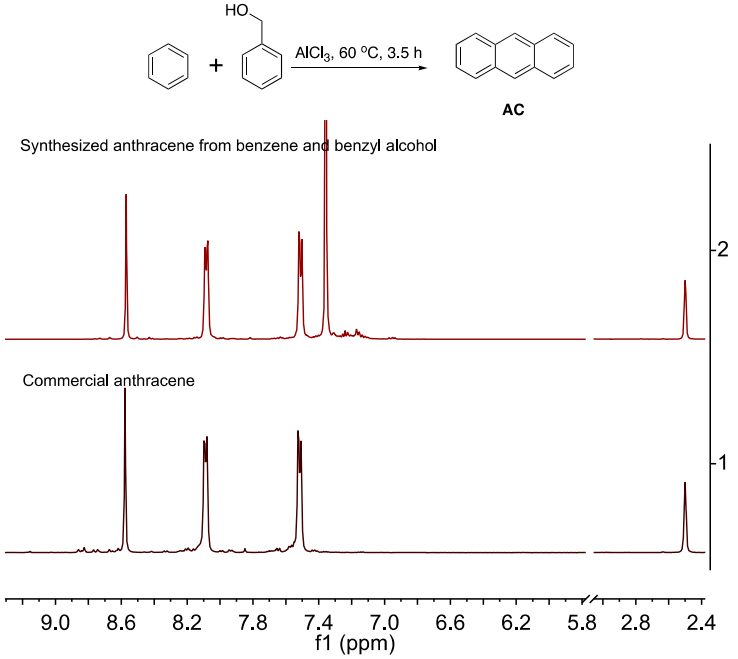

Figure S16. ^{1}H NMR spectra of commercial and synthesized anthracene (**AC**) in DMSO-d_6. The peak at 7.37 ppm in the synthesized **AC** spectrum is from benzene.

REFERENCES

S1 H.-J. Schäfer, *Topics in Current Chemistry*, 1990, **152**, 91–151.

S2. G. Maier, L. H. Franz, H.-G. Hartan, K. Lanz and H. P. Reisenauer, *Chemische Berichte*, 1985, **118**, 3196–3204.

S3. B. E. Hulme, E. J. Land and G. O. Phillips, *J. Chem. Soc. Faraday Trans. 1*, 1972, **68**, 1992–2002.

S4. S. A. Carlson and D. M. Hercules, *Analytical Chemistry*, 1973, **45**, 1794–1799.

S5. D. M. Hercules, S. A. Carlson, *Analytical Chemistry* 1974**, 46**, 674–678.

S6. A. D. Broadbent, R. P. Newton, *Canadian Journal of Chemistry* 1972**, 50**, 381–387.